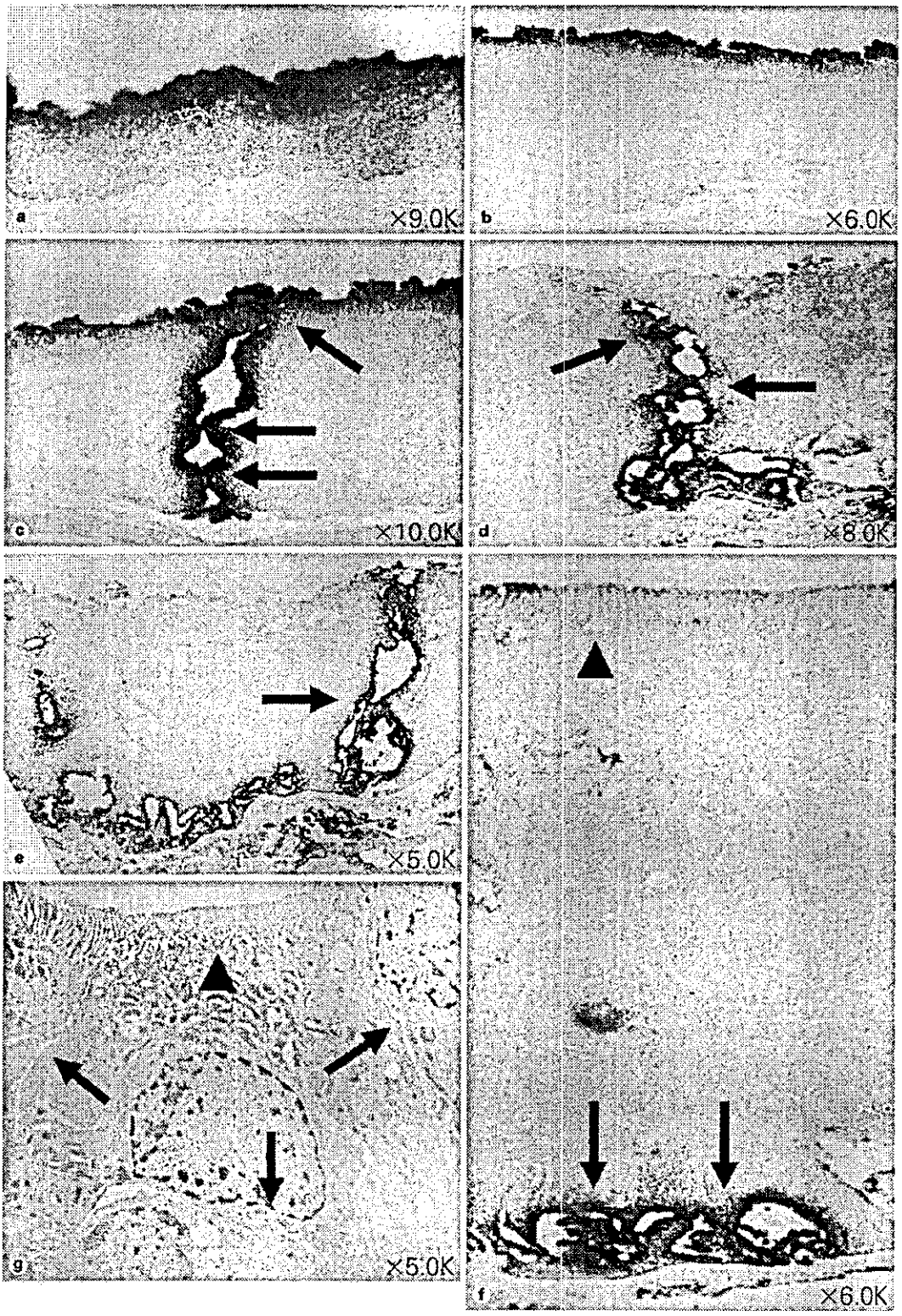
a
×9.0K
b
×6.0K
c
×10.0K
d
×8.0K
e
×5.0K
g
×5.0K
f
×6.0K

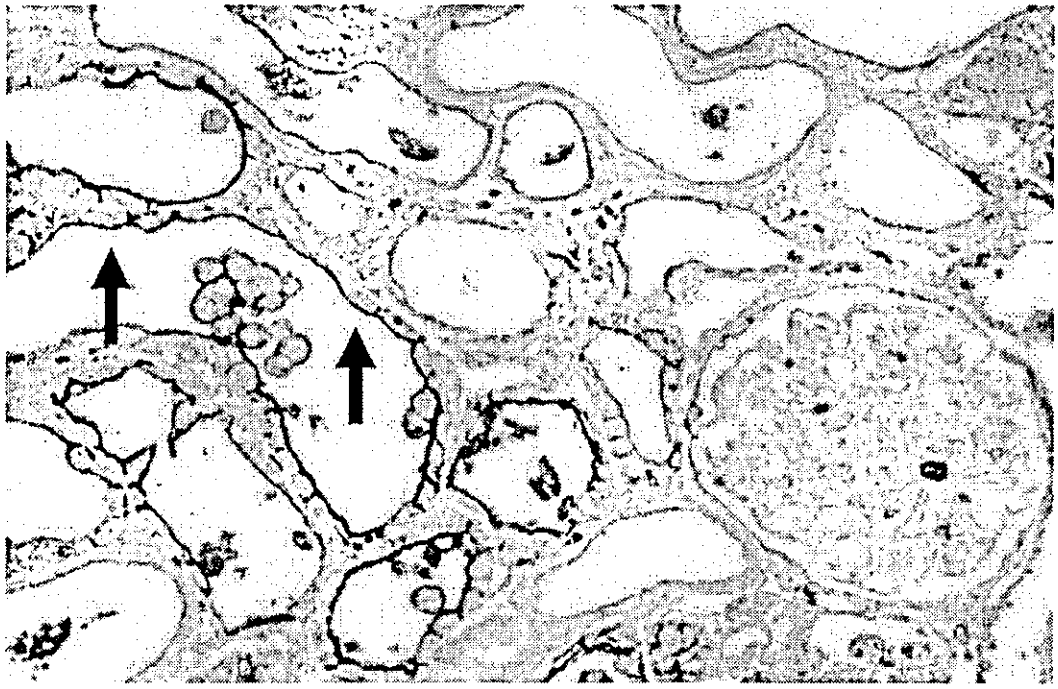

Fig. 3. Colocalization of CD44-OX49 on the apical surface membrane and proliferating cell nuclear antigen (PCNA) in the recovery stage after acute tubular necrosis. Note that the CD44-OX49-positive (brown) cells on the apical surface membrane are mainly PCNA-positive (red) cells, that is, newly regenerative tubular epithelial cells on day 10 after the first gentamicin injection. Original magnification × 100.

Colocalization of CD44-OX49 on the Apical Surface Membrane and PCNA

We demonstrated previously that the regeneration of tubular epithelial cells was most marked on day 10 after the first gentamicin injection. That is, the number of cortical tubular PCNA-positive cells reached a peak on day 10 [9]. To establish whether CD44-OX49-positive cells on the apical surface membrane were newly regenerative tubular epithelial cells or not, we carried out double staining for CD44-OX49 and PCNA as a regenerative marker. The result showed that the CD44-OX49-positive cells on the apical surface membrane were mainly PCNA-positive cells, that is, newly regenerative cells in the tubular epithelia, especially on day 10 after the first gentamicin injection (fig. 3).

Distribution of CD44-OX49 on the Plasma Membrane in Tubular Epithelium

In order to clarify the distribution of CD44 on epithelial cell PM in distinct stages in the gentamicin-induced ATN and recovery process, we performed quantitative analysis for localization of CD44-OX49 on tubular epithelial cell PM. The results showed that staining for CD44-OX49 was negative in full necrotic tubules on day 6 after the first gentamicin injection. On day 10, CD44-OX49 was positive on the apical PM in 68 tubules, lateral PM in 38 tubules and basal PM in 15 tubules, respectively, in 100 PCNA-positive and CD44-OX49-positive tubules. On day 15, CD44-OX49 was positive on the apical PM in 36 tubules, lateral PM in 82 tubules and basal PM in 34 tubules, respectively, in 100 CD44-OX49-positive tubules. On day 30, CD44-OX49 was positive on the apical PM in 12 tubules, lateral PM in 42 tubules and basal PM in 64 tubules, respectively, in 100 CD44-OX49-positive tubules. That is, CD44-OX49 was mainly localized to the apical PM in the early recovery stage, the lateral PM in the middle recovery stage and the basal PM in the late recovery stage after ATN (fig. 4).

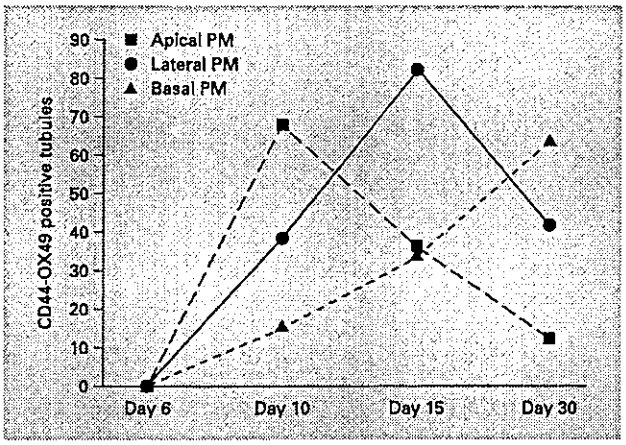

Fig. 4. Distribution of CD44-OX49 on the epithelial cell plasma membrane (PM) at distinct stages after acute tubular necrosis. Observations were performed on 100 non-overlapping random tubules 20 per rat kidney section from 5 rats at day 6, 10, 15 and 30 after the first gentamicin administration. The number of CD44-OX49 positive stained tubules with stained cells greater than 50% of PM was recorded. If both the basolateral PM and the apical PM were stained in greater than 50% cells these were recorded separately as basolateral PM positive and apical PM positive. Note that the CD44-OX49 is mainly localized to the apical PM in the early recovery stage, the lateral PM in the middle recovery stage and the basal PM in the late recovery stage after ATN.

Discussion

Previous in vitro studies have demonstrated that in polarized epithelial cells, a tailless CD44 molecule is localized on the apical PM, whereas wild-type CD44 is restricted to the lateral-basal PM of epithelial cells [7]. However, in vivo studies demonstrated that CD44 is generally localized on the lateral-basal PM of renal tubular polarized epithelial cells in the kidneys, but whether it is localized on the apical PM of epithelial cells is unclear [8]. Our present in vivo study showed that CD44 was localized on not only the lateral-basal PM of renal tubular polarized epithelial cells, but also the apical PM. The staining for CD44-OX49 was positive on the apical PM in newly regenerative tubular epithelial cells in the early recovery stages after ATN, whereas staining for CD44CPT was negative. CD44CPT was only located on the lateral-basal PM. These results suggest that there were at least two types of CD44 during regeneration and repair processes after ATN. One was CD44 without a cytoplasmic tail localizing on the apical surface membrane in newly regenerative epithelial cells. Another was CD44 with a cytoplasmic tail localizing on the lateral-basal PM. Lewington et al. [8] reported that there were 4 transcripts of CD44 mRNA (4.5, 3.3, 2.0 and 1.6 kb) in kidney after acute ischemic injury in rats by Northern blot analysis. In this study, we did not perform Northern blot or Western blot analysis of CD44 because our previous study demonstrated that CD44 was located not only in renal tubular epithelial cells, but also in monocytes/macrophages in injury kidneys [9] and general Western blot could not distinguish CD44 located in renal tubules or CD44 located in monocytes/macrophages.

Both CD44 localized on the apical PM and on the lateral-basal PM were positive for immunohistochemical staining with a purified mouse anti-rat CD44-OX49 monoclonal antibody, which indicated both CD44 localized on the apical PM and CD44 localized on the lateral-basal PM might have same epitope in their distal extracellular domains. The epitope recognized by the CD44-OX49 antibody has been mapped to a region on both the standard CD44 and the splice variant isoforms of CD44 [11].

In vitro studies have demonstrated that as polarized MDCK epithelial cell cultures reach confluency, CD44 is excluded from the apical surface and becomes concentrated at areas of cell contact along the lateral cell surfaces. Additionally, in MDCK epithelial cells, both the endogenous and transfected wild-type CD44 were found on the lateral-basal surface. Deletion of the CD44 cytoplasmic tail reduces the half-life of this mutant protein and causes it to be expressed on the apical surface [7]. Confocal microscopy studies showed that CD44 indeed is expressed at the apical surface of subconfluent cultures of proximal and distal human tubular kidney cells on day 5. However, on day 9, CD44 had disappeared from the apical surface and translocated to the lateral-basal membrane [12]. These in vitro results suggest that the localization of CD44 may be regulated, and that the CD44 localized on the apical PM of epithelial cells may be CD44 without cytoplasmic domain. They may be a product of immature cells at an early stage of cell development and with a short half life. However, it has not been elucidated whether CD44 is expressed on the apical PM of epithelial cells in vivo. Our in vivo study revealed that CD44-OX49 was distinctly localized on the apical surface membrane in PCNA-positive newly regenerative epithelial cells in the early recovery stage after ATN, suggesting that it is possibly related to the regeneration of renal tubular epithelial cells. Our previous study demonstrated that a CD44 ligand, osteopontin, is related to regeneration of epithelial cells after ATN [9], this role of osteopontin might be achieved by CD44. Many studies showed that CD44

could be related to cell proliferation, regeneration and repair of injured tissues. In the facial nucleus after nerve injury and during the ensuing regeneration, strong up-regulation of CD44 on the regenerating motoneurons in the axotomized facial nucleus suggests that CD44 play a role in neurite outgrowth [13]. In the remodeling phase of healing of fractures, intense CD44 and OPN were detected in osteocytes and osteocyte lacunae, suggesting that CD44 bound to OPN plays a role in the repair of skeletal tissues [14]. In a partial hepatectomy model for studying cellular proliferation, CD44 influenced cellular differentiation, growth, cell-cell interactions and cellular polarity, and played an important role in the proliferation of residual hepatocytes and the liver regeneration [15].

Concerning localization of CD44 on lateral-basal PM, in vitro studies showed that lateral-basal targeting signals of membrane protein were localized in the cytoplasmic domain near the plasma membrane in a number of cases [1]. Mutational studies have identified His^{330}-Lys^{334} in the cytoplasmic domain (Asn^{290}-Val^{361}) of human CD44 as a localization signal that directs membrane proteins to the lateral-basal surface. This sorting signal appears to depend critically on the integrity of the dipeptide Leu^{331} and Val^{332}. That is, mutation of Leu^{331} generated a mutant protein that was expressed on the apical PM, and mutation of Val^{332} resulted in the majority of the protein being located to the lateral surface of the cells, with a residual proportion observed at the apical surface [2, 16]. However, whether or not the CD44 localized on lateral-basal PM is CD44 with a cytoplasmic domain in vivo is not clear. The present study, in which the CD44CPT was only observed at the lateral-basal PM, but not at the apical PM, confirmed for the first time that CD44 localized on the lateral-basal PM of renal tubular epithelial cells was CD44 with a cytoplasmic domain in vivo.

Although the specific mechanism was not clear, the functional significance of CD44 on the lateral-basal PM may be related to the establishment of tubular epithelial cell polarity during the recovery process after ATN. This was because adhesion and the cytoskeleton play an important role in establishment of cell polarity, and because CD44 is closely related to adhesion and the cytoskeleton. In epithelial cells, extrinsic cues from cell-cell adhesion result in the formation of cytoskeletal and signaling networks at cell contacts resulting in partial reorganization of the cells. However, full establishment of epithelial cell polarity requires both cell-cell and cell-ECM (extracellular matrix) adhesion. Specialized cytoskeletal and signaling networks assemble around adhesion receptors and position other cytoskeletal complexes and protein-sorting compartments relative to the spatial cue. In addition, binding of the cytoskeleton to adhesion receptors strengthens cell adhesion and maintains signaling from the cues [17]. The CD44 proteins are cell surface adhesion molecules involved in cell-cell and cell-matrix interactions. The principal ligand of CD44 is hyaluronic acid, an integral component of the ECM. Other CD44 ligands include osteopontin, serglycin, collagens, fibronectin, and laminin [4]. Kalomiris and Bourguignon [18] demonstrated that CD44 is a transmembrane protein with a cytoplasmic domain that binds directly to ankyrin, a molecule known to link the membrane to the cytoskeleton. Ankyrin plays a specific role in membrane skeleton organization, ionic transport, and maintenance of cell polarity, as well as cell-cell adhesion regulation. The interaction between the membrane skeleton and cytoplasmic domains of transmembrane proteins plays a fundamental role in membrane integrity and stability, as well as in many other cellular processes [19]. In addition, the CD44 cytoplasmic domain also can directly bind to ERM family members (ezrin, radixin, and moesin), which are crucial components that provide a regulated linkage between membrane proteins and the cortical cytoskeleton, as well as participating in signal-transduction pathways [6, 20, 21]. Our in vivo results showed that CD44 was expressed distinctly on the lateral PM and in close contact with lateral PM between cells (cell-cell adhesion) in the middle stage of epithelial cell repair after ATN. In the late stage of epithelial cell repair, CD44 was mainly located to the basal PM. By that time, epithelial cell polarity had been basically established, evidenced by initial microvilli appearance in the apical surface membrane. After full establishment of epithelial cell polarity, CD44 disappeared from the basal surface membrane. These results suggest CD44 is related to the establishment of epithelial cell polarity.

In summary, we used a gentamicin-induced ATN and spontaneous recovery model in rats and two distinct antibodies and surveyed the localization of CD44-OX49 and CD44CPT on the PM in renal tubular epithelial cells in the recovery process after ATN with immunohistochemistry and immunoelectron-microscopic examination. The present study provided the following new in vivo evidence. First, CD44-OX49 was localized not only on the lateral-basal PM of renal tubular epithelial cells, but also on the apical PM in PCNA-positive newly regenerative tubular epithelial cells in the early recovery stages after ATN, whereas CD44CPT was localized only on the lateral-basal PM in vivo. Second, localization of CD44 was changed from the apical to lateral to basal PM in renal tubular epithelial cells during the recovery process after

ATN, and finally disappeared from the basal surface membrane when normal polarized epithelial cells formed in vivo. These results suggest that there were two types of CD44, with and without a cytoplasmic tail, with different localization during the recovery process after ATN. The CD44 localized on the apical surface membrane might have been CD44 without a cytoplasmic tail which could be related to the regeneration of epithelial cells, whereas the CD44 localized on the lateral and basal PM might have been CD44 with a cytoplasmic tail which could participate in establishment of tubular epithelial cell polarity by adhesion and binding of cytoskeletal associated proteins.

Acknowledgements

This work was supported in part by a Health and Labour Science Research Grant for Research on Specific Diseases from the Ministry of Health, Labour and Welfare, and by a Grant-in-Aid for Scientific Research (C, No. 11671032) from the Ministry of Education, Culture, Sports, Science and Technology of Japan. An abstract of this work was presented at the 44th Annual Meeting of the Japanese Society of Nephrology (Tokyo, Japan, 2001) and the 2001 ASN/ISN World Congress of Nephrology (San Francisco, Calif., USA, 2001), respectively.

References

1 Matter K, Mellman I: Mechanisms of cell polarity: Sorting and transport in epithelial cells. Curr Opin Cell Biol 1994;6:545–554.
2 Sheikh H, Isacke CM: A di-hydrophobic Leu-Val motif regulates the lateral-basal localization of CD44 in polarized Madin-Darby canine kidney epithelial cells. J Biol Chem 1996;271: 12185–12190.
3 Xie Y, Sakatsume M, Nishi S, Narita I, Arakawa M, Gejyo F: Expression, roles, receptors, and regulation of osteopontin in the kidney. Kidney Int 2001;60:1645–1657.
4 Goodison S, Urquidi V, Tarin D: CD44 cell adhesion molecules. Mol Pathol 1999;52:189–196.
5 Lesley J, Hyman R: CD44 structure and function. Front Biosci 1998;3:D616–630.
6 Tsukita S, Oishi K, Sato N, Sagara J, Kawai A, Tsukita S: ERM family members as molecular linkers between the cell surface glycoprotein CD44 and actin-based cytoskeletons. J Cell Biol 1994;126:391–401.
7 Neame SJ, Isacke CM: The cytoplasmic tail of CD44 is required for lateral-basal localization in epithelial MDCK cells but does not mediate association with the detergent-insoluble cytoskeleton of fibroblasts. J Cell Biol 1993;121: 1299–1310.
8 Lewington AJ, Padanilam BJ, Martin DR, Hammerman MR: Expression of CD44 in kidney after acute ischemic injury in rats. Am J Physiol 2000;278:R247–R254.
9 Xie Y, Nishi S, Iguchi S, Imai N, Sakatsume M, Saito A, Ikegame M, Iino N, Shimada H, Ueno M, Kawashima H, Arakawa M, Gejyo F: Expression of osteopontin in gentamicin-induced acute tubular necrosis and its recovery process. Kidney Int 2001;59:959–974.
10 Gunthert U, Hofmann M, Rudy W, Reber S, Zoller M, Haussmann I, Matzku S, Wenzel A, Ponta H, Herrlich P: A new variant of glycoprotein CD44 confers metastatic potential to rat carcinoma cells. Cell 1991;65:13–24.
11 Arch R, Wirth K, Hofmann M, Ponta H, Matzku S, Herrlich P, Zoller M: Participation in normal immune responses of a metastasis-inducing splice variant of CD44. Science 1992; 257:682–685.
12 Verhulst A, Asselman M, Persy VP, Schepers MS, Helbert MF, Verkoelen CF, De Broe ME: Crystal retention capacity of cells in the human nephron: Involvement of CD44 and its ligands hyaluronic acid and osteopontin in the transition of a crystal binding into a nonadherent epithelium. J Am Soc Nephrol 2003;14:107–115.
13 Jones LL, Kreutzberg GW, Raivich G: Regulation of CD44 in the regenerating mouse facial motor nucleus. Eur J Neurosci 1997;9:1854–1863.
14 Yamazaki M, Nakajima F, Ogasawara A, Moriya H, Majeska RJ, Einhorn TA: Spatial and temporal distribution of CD44 and osteopontin in fracture callus. J Bone Joint Surg Br 1999;81:508–515.
15 Della Fazia MA, Pettirossi V, Ayroldi E, Riccardi C, Magni MV, Servillo G: Differential expression of CD44 isoforms during liver regeneration in rats. J Hepatol 2001;34:555–561.
16 Stamenkovic I, Amiot M, Pesando JM, and Seed B: A lymphocyte molecule implicated in lymph node homing is a member of the cartilage link protein family. Cell 1989;56:1057–1062.
17 Drubin DG, Nelson WJ: Origins of cell polarity. Cell 1996;84:335–344.
18 Kalomiris EL, Bourguignon LY: Mouse T lymphoma cells contain a transmembrane glycoprotein (GP85) that binds ankyrin. J Cell Biol 1988;106:319–327.
19 Hryniewicz-Jankowska A, Czogalla A, Bok E, Sikorsk AF: Ankyrins, multifunctional proteins involved in many cellular pathways. Folia Histochem Cytobiol 2002;40:239–249
20 Nakamura H, Ozawa H: Immunolocalization of CD44 and the ERM family in bone cells of mouse tibiae. J Bone Miner Res 1996;11:1715–1722.
21 Nakamura H, Ozawa H: Immunolocalization of CD44 and the ezrin-radixin-moesin (ERM) family in the stratum intermedium and papillary layer of the mouse enamel organ. J Histochem Cytochem 1997;45:1481–1492.

THE JOURNAL OF BIOLOGICAL CHEMISTRY
Vol. 279, No. 7, Issue of February 13, pp. 6017–6026, 2004
Printed in U.S.A.

Caffeic Acid Phenethyl Ester Induces Apoptosis by Inhibition of NFκB and Activation of Fas in Human Breast Cancer MCF-7 Cells*

Received for publication, June 9, 2003, and in revised form, October 27, 2003
Published, JBC Papers in Press, November 18, 2003, DOI 10.1074/jbc.M306040200

Masahiko Watabe‡, Keiichi Hishikawa§¶, Atsushi Takayanagi‖, Nobuyoshi Shimizu‖, and Toshio Nakaki‡

From the ‡Department of Pharmacology, Teikyo University School of Medicine, Tokyo 173-8605, the §Department of Clinical Renal Regeneration, Graduate School of Medicine, University of Tokyo, Tokyo 113-8655, and the ‖Department of Molecular Biology, Keio University School of Medicine, Tokyo 160-8582, Japan

The transcription factor NFκB plays a role in cell survival. Apoptosis, programmed cell death, via numerous triggers including death receptor ligand binding is antagonized by NFκB activation and potentiated by its inhibition. In the present study, we found that caffeic acid phenethyl ester (CAPE), known to inhibit NFκB, induced apoptosis via Fas signal activation in human breast cancer MCF-7 cells. CAPE activated Fas by a Fas ligand (Fas-L)-independent mechanism, induced p53-regulated Bax protein, and activated caspases. CAPE also activated MAPK family proteins p38 and JNK. SB203580, a specific inhibitor of p38 MAPK, partially suppressed CAPE-induced p53 activation, Bax expression, and apoptosis, consistent with a mechanism by which CAPE leads to Bax activation, known to be regulated by p38 and p53. The expression of dominant negative c-Jun, which inhibits the JNK signal, also suppresses CAPE-induced apoptosis, suggesting MAPKs are involved in CAPE-induced apoptosis. The expression of Fas antisense oligomers significantly suppressed the CAPE-induced activations of JNK and p38 and apoptosis as compared with Fas sense oligomers. To ascertain whether these phenomena are attributable to the inhibition of NFκB by CAPE, we examined the effect of a truncated form of IκBα (IκBΔN) lacking the phosphorylation sites essential for NFκB activation. IκBΔN expression not only inhibited NFκB activity but also induced Fas activation, Bax expression, and apoptosis. Our findings demonstrate that NFκB inhibition is sufficient to induce apoptosis and that Fas activation plays a role in NFκB inhibition-induced apoptosis in MCF-7 cells.

Programmed cell death can occur in all cells by highly efficient mechanisms, leading to the quiet disposal of millions of cells in the adult human. This efficient removal of unnecessary cells is regulated not only by cell death signals but also by those of cell survival. Any imbalance between these signals can be lethal in the development of higher organisms and likely plays a major role in pathophysiological processes as diverse as atherosclerosis, heart failure, and inflammation.

Originally defined as a nuclear factor that binds to the B site of the immunoglobulin κ light chain gene enhancer in B lymphocytes (1), transcription factor NFκB is crucial for the inducible expression of many genes involved in immunity and inflammation (2). NFκB is a member of the rel multigene family and comprises five major proteins: p50, p65 (RelA), c-rel, p52, and RelB (3). The most abundant form of NFκB is the heterodimer of p50 and p65 that is retained in the cytosol by specific inhibitory proteins termed IκB (2). IκB kinases are central to NFκB activation (4–6). The IκB kinases trigger the phosphorylation of IκB on amino-terminal serine residues 32 and 36, upon which the conjugation of ubiquitin occurs, and then targets the phosphorylated IκB for degradation by proteasomes (6). The released nucleophilic heterodimer then moves to the nucleus, where both p50 and p65 contribute to NFκB DNA binding (3). The p65 subunit is responsible for transcriptional activity, resulting in the expression of NFκB-responsive target genes. Caffeic acid phenethyl ester (CAPE),[1] a structural derivative of flavonoids, is a biologically active ingredient of honeybee propolis and a potent and specific inhibitor of NFκB activation (7).

In this study we found that CAPE, which is known to inhibit NFκB, activates the Fas death receptor in human breast cancer MCF-7 cells. We demonstrate herein that CAPE not only inhibits NFκB activity but also activates Fas in a Fas-L-independent manner. Moreover, CAPE induces Bax expression, caspase activation, DNA fragmentation, and apoptosis. We used a truncated form of IκBα (IκBΔN) lacking the phosphorylation sites essential for NFκB activation as an alternative method of inhibiting this activation. IκBΔN expression caused phenomena qualitatively identical to those observed with CAPE treatment. Taken together, these findings suggest that NFκB inhibition is sufficient to activate Fas death receptors and to induce apoptosis in human breast cancer cells.

MATERIALS AND METHODS

Materials—Anti-actin antibody, *N*-benzyloxycarbonyl-Val-Ala-Asp-(OMe) fluoromethyl ketone (Z-VAD-FMK), Z-Leu-Glu(OMe)-Thr-Asp(OMe)-fluoromethyl ketone (Z-IETD-FMK), Z-Leu-Glu(OME)-His-Asp(OMe) fluoromethyl ketone (Z-LEHD-FMK), and recombinant Fas-L (soluble) were purchased from Sigma. Anti-active JNK antibody and anti-active p38 antibody were from Promega. Polyclonal anti-Fas, Fas-L, Bax, and Fas-associated death domain (FADD) antibody were from Santa Cruz Biotechnology. 3,3′-Dithiobis(sulfosuccinimidyl-propionate) was from Pierce. Fas ligand inhibitor was from Kamiya Biomedical Company.

Cell Culture—MCF-7 cells were grown in Dulbecco's modified Ea-

* This work was supported in part by The Naito Foundation. The costs of publication of this article were defrayed in part by the payment of page charges. This article must therefore be hereby marked "*advertisement*" in accordance with 18 U.S.C. Section 1734 solely to indicate this fact.

¶ To whom correspondence should be addressed: Dept. of Clinical Renal Regeneration, Graduate School of Medicine, University of Tokyo 113-8655. Tel.: 81-3-3815-5411 (ext. 35725); Fax: 81-3-5800-9738; E-mail: hishikawa-tky@umin.ac.jp.

[1] The abbreviations used are: CAPE, caffeic acid phenethyl ester; JNK, c-Jun NH_2-terminal kinase; MAPK, mitogen-activated protein kinase; Fas-L, Fas ligand; FMK, fluoromethyl ketone; FADD, Fas-associated death domain; m.o.i., multiplicity of infection; GFP, green fluorescent protein.

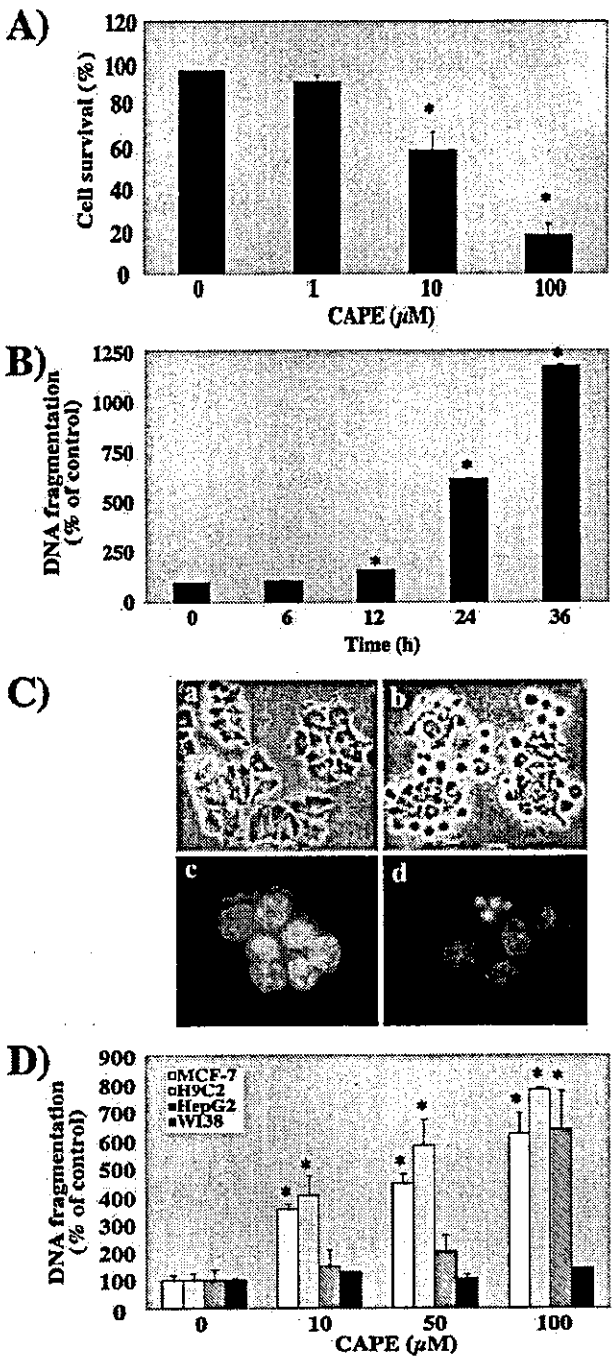

FIG. 1. **CAPE-induced apoptosis.** *A*, MCF-7 cells were treated with CAPE at the indicated concentrations for 48 h. Cell viability was determined by trypan blue exclusion assay. *B*, MCF-7 cells were treated with 10 μM CAPE for the indicated times. DNA fragmentation assay was performed as described under "Materials and Methods." *C*, MCF-7 cells were treated without (*a*, *c*) or with (*b*, *d*) 10 μM CAPE for 48 h. Morphological changes in cells were examined by phase-contrast microscopy (*a*, *b*) and by staining with Hoechst 33258 (*c*, *d*). *D*, MCF-7, H9C2, HepG2,and WI-38 cells were treated with CAPE at the indicated concentrations for 24 h. DNA fragmentation assay was performed as described for *panel B*. Results are presented as the means ± S.E. of three independent experiments. *, $p < 0.05$ compared with 10 μM CAPE.

gle's medium supplemented with 10% fetal calf serum at 37 °C under 5% CO_2 in air.

DNA Fragmentation—DNA fragmentation was measured using a

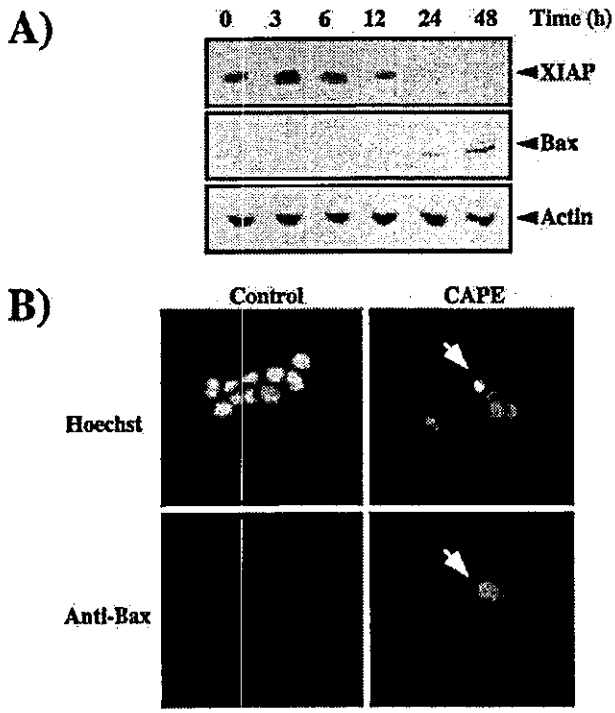

FIG. 2. **Effects of CAPE on the expression of apoptosis-related proteins.** *A*, MCF-7 cells were treated with 10 μM CAPE for the indicated times. After cell lysate preparation, immunoblotting analyses were performed using specific antibodies. *B*, MCF-7 cells were treated with 10 μM CAPE for 24 h. Intracellular localization of Bax protein was examined by immunofluorescence microscopy.

cell death detection ELISA^{PLUS} kit (Roche Molecular Biochemicals) according to the manufacturer's instructions.

Nuclear Morphology—Morphological study was performed as described previously (8). After CAPE treatment, the cells were collected, washed with phosphate-buffered saline, fixed with 3.7% formaldehyde for 20 min, and incubated in 2 μg/ml Hoechst33258 (Sigma) for 5 min. Nuclear morphology was examined using fluorescence microscopy.

Immunoblot Analysis—Immunoblotting was performed as described previously (9). Cells were lysed in buffer containing SDS and mercaptoethanol, and the cell lysate was then boiled. Denatured proteins were separated on a polyacrylamide gel and transferred to a polyvinylidene difluoride membrane (Amersham Biosciences). The membrane was incubated with a blocking solution (2% skim milk (Invitrogen) dissolved in phosphate-buffered saline containing 0.2% Tween 20 (TPBS) for 1 h at room temperature, washed with TPBS, and incubated for 1 h with a primary antibody dissolved in the blocking solution overnight at 4 °C. After washing, the membrane was incubated for 1 h with the respective horseradish-linked secondary antibody. Immunoreactive proteins were detected with an enhanced chemiluminescence system (Amersham Biosciences) and analyzed with image analysis software NIH-Image 1.62 for the Macintosh.

Immunofluorescence Microscopy—Immunocytochemical study was performed as described previously (10, 11). Cells were washed with phosphate-buffered saline and fixed with 3.7% formaldehyde for 20 min. Cells were permeabilized with phosphate-buffered saline containing 0.2% Triton X-100 for 5 min and then washed three times with phosphate-buffered saline. Incubation with primary antibody was carried out for 1 h at room temperature. Excess antibody was washed three times with phosphate-buffered saline. This was followed by incubation with an appropriate fluorophore-labeled secondary antibody for 1 h at room temperature in an area protected against light. After washing out the excess antibody three times with phosphate-buffered saline, we performed a mounting operation with phosphate-buffered saline containing 1 μg/ml Hoechst33258 (Sigma). Images were collected by fluorescence microscopy.

Reporter Assay—Reporter assays were performed as described previously (12). Twenty-four hours after co-transfection with p3xκB-Luc or p53-Luc (Stratagene) and pRL-TK (Promega) using SuperFect™ (Qiagen), the cells were treated with CAPE. Transcriptional activity in CAPE-treated cells was measured as the enzyme activity of luciferase,

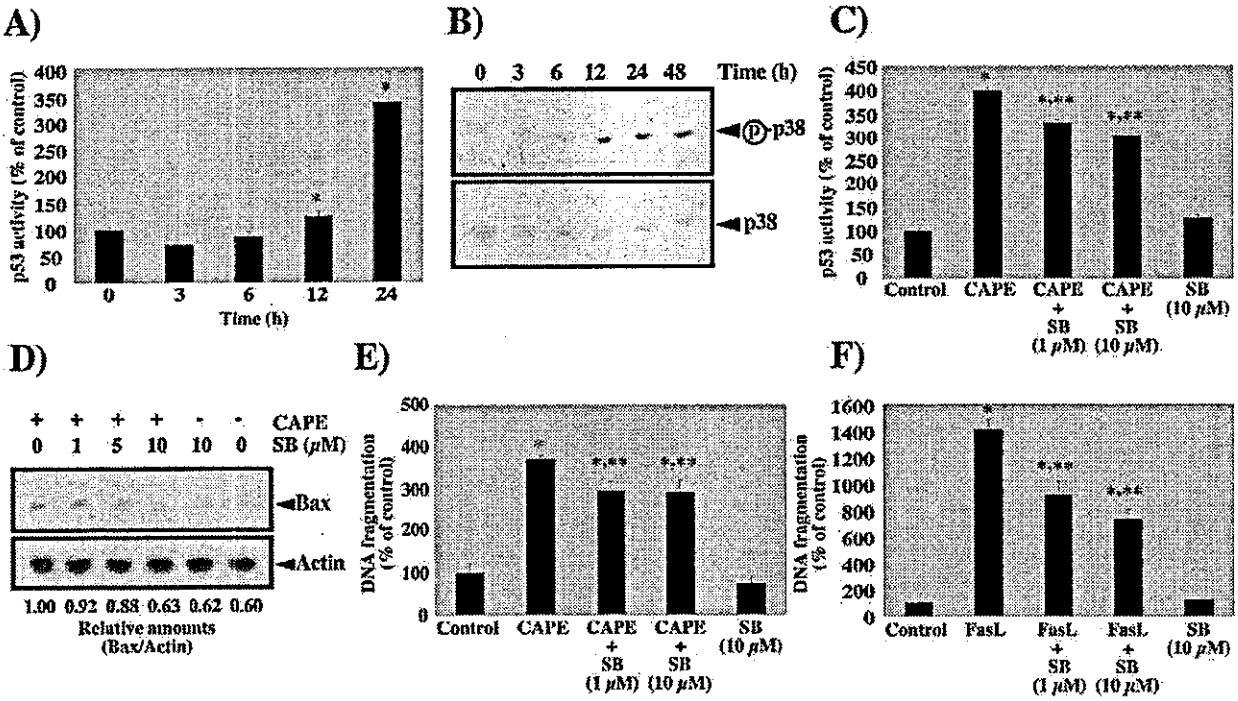

FIG. 3. **p38 involvement in CAPE-induced apoptosis.** MCF-7 cells were treated with 10 μM CAPE for the indicated times. *A*, transcriptional activity of p53 was measured as described under "Materials and Methods." Results are presented as the means ± S.E. of three independent experiments. *, $p < 0.05$ compared with control. *B*, after cell lysate preparation, immunoblotting analyses were performed using anti-p38 and phospho-p38 antibodies. After MCF-7 cells had been pretreated with SB203580 for 30 min at the indicated concentration, they were treated with 10 μM CAPE for 24 h. *C*, transcriptional activity of p53 was measured as in *panel A*. Results are presented as the means ± S.E. of three independent experiments. *, $p < 0.05$ compared with control. **, $p < 0.05$ compared with CAPE alone. *D*, after cell lysate preparation, immunoblotting analysis was performed using anti-Bax and actin antibodies. The quantitative analysis was performed and the expressed amounts of Bax were normalized with actin. *E*, DNA fragmentation assay was performed as described under "Materials and Methods." Results are presented as the means ± S.E. of three independent experiments. *, $p < 0.05$ compared with control. **, $p < 0.1$ compared with CAPE alone. *F*, after MCF-7 cells had been pretreated with SB203580 for 30 min at the indicated concentration, they were treated with 5 ng/ml recombinant Fas-L for 24 h. DNA fragmentation assay was performed as in *panel E*. Results are presented as the means ± S.E. of three independent experiments. *, $p < 0.05$ compared with control. **, $p < 0.05$ compared with Fas-L alone.

which is a product of the reporter gene, using a dual-luciferase reporter assay system (Promega).

Fas Cross-linking and Immunoprecipitation—Immunoprecipitation was performed as described previously (13, 14). After treatment with CAPE, the cells were pelleted, washed twice in phosphate-buffered saline, resuspended in phosphate-buffered saline, and treated with 2 mM cross-linker 3,3′-dithiobis(sulfosuccinimidylpropionate) for 15 min on ice. The reaction was quenched with 10 mM ammonium acetate for 10 min. The cells were pelleted, washed twice in phosphate-buffered saline, and lysed in lysis buffer (20 mM Tris-Cl (pH 7.4), 140 mM NaCl, 10% glycerol, 1% Triton X-100, and 2 mM EDTA) containing a protease inhibitor mixture (Roche Molecular Biochemicals). The cell lysates were then used for immunoprecipitation in the presence of an anti-Fas antibody at 0.5 μg/ml (antibody limiting) or 10 μg/ml (antibody excess). Immune complexes were precipitated using protein A/G PLUS-agarose (Santa Cruz Biotechnology) and washed four times in lysis buffer. The precipitate was resuspended in buffer containing SDS and mercaptoethanol, boiled, and then immunoblot analysis was performed.

Detection of Fas-FADD Complex—Using an immunoprecipitation method, the Fas-FADD complex was detected as described previously (13, 14). After treatment with CAPE, the cells were pelleted, washed twice in phosphate-buffered saline, resuspended in phosphate-buffered saline, and treated with 2 mM cross-linker 3,3′-dithiobis(sulfosuccinimidylpropionate) for 15 min on ice. The reaction was quenched with 10 mM ammonium acetate for 10 min. The cells were pelleted, washed twice in phosphate-buffered saline, and lysed in lysis buffer (20 mM Tris-Cl (pH 7.4), 140 mM NaCl, 10% glycerol, 1% Triton X-100, and 2 mM EDTA) containing a protease inhibitor mixture. The cell lysates were then used for immunoprecipitations in the presence of an anti-Fas antibody. Immune complexes were precipitated using protein A/G PLUS-agarose and washed four times in lysis buffer. The precipitate was resuspended in buffer containing SDS and mercaptoethanol, boiled, and then immunoblotted. Half the immunoprecipitate was used for immunoblot analysis to detect the presence of FADD, and the other half was used to detect the presence of Fas.

Blockage of Fas Signaling with Fas Antisense Oligonucleotides—For antisense experiments, MCF-7 cells were transiently transfected with sense or antisense Fas oligonucleotides using SuperFect™ (Qiagen) in accordance with the manufacturer's manual. After 24 h of transfection, the cells were treated with CAPE. Oligomer sequences for Fas sense (ATG CTG GGC ATC TGG ACC CTC) and antisense (GAG GGT CCA GAT GCC CAG CAT) oligonucleotides were directed against the ATG translation start site in Fas mRNA and were modified with phosphorothioate (Invitrogen).

Recombinant Adenovirus Vector and Transfection Efficiency—We constructed a recombinant adenovirus vector expressing the non-degraded form of the NFκB inhibitor IκBα as described previously (15). This nondegraded IκBα (IκBΔN) lacks the NH_2-terminal 54 amino acids of wild type human IκBα. IκBΔN is reportedly not phosphorylated or proteolyzed in response to signal induction but does fully inhibit NFκB (16). To evaluate the efficiency of adenovirus-mediated gene transfer, cells were incubated with AdexlacZ at 37 °C using different multiplicities of infection (m.o.i., 1, 10, 50, and 100). β-galactosidase expression was evaluated by X-gal staining. After 48 h of incubation, AdexlacZ-infected cells were fixed with 1% glutaraldehyde in 0.1 M sodium phosphate (pH 7.0) and 1 mM $MgCl_2$ for 15 min. Cells were washed with phosphate-buffered saline and assayed for lacZ expression by the X-gal staining method (15). Transfection efficiency was increased in an m.o.i.-dependent manner and reached ~70% at an m.o.i. of 100 (data not shown). We therefore employed an m.o.i. of 100 in all of the experiments.

RESULTS

CAPE-induced Apoptosis—We first examined the effect of CAPE on cell viability in human breast cancer MCF-7 cells. CAPE treatment for 48 h decreased cell viability in a dose-de-

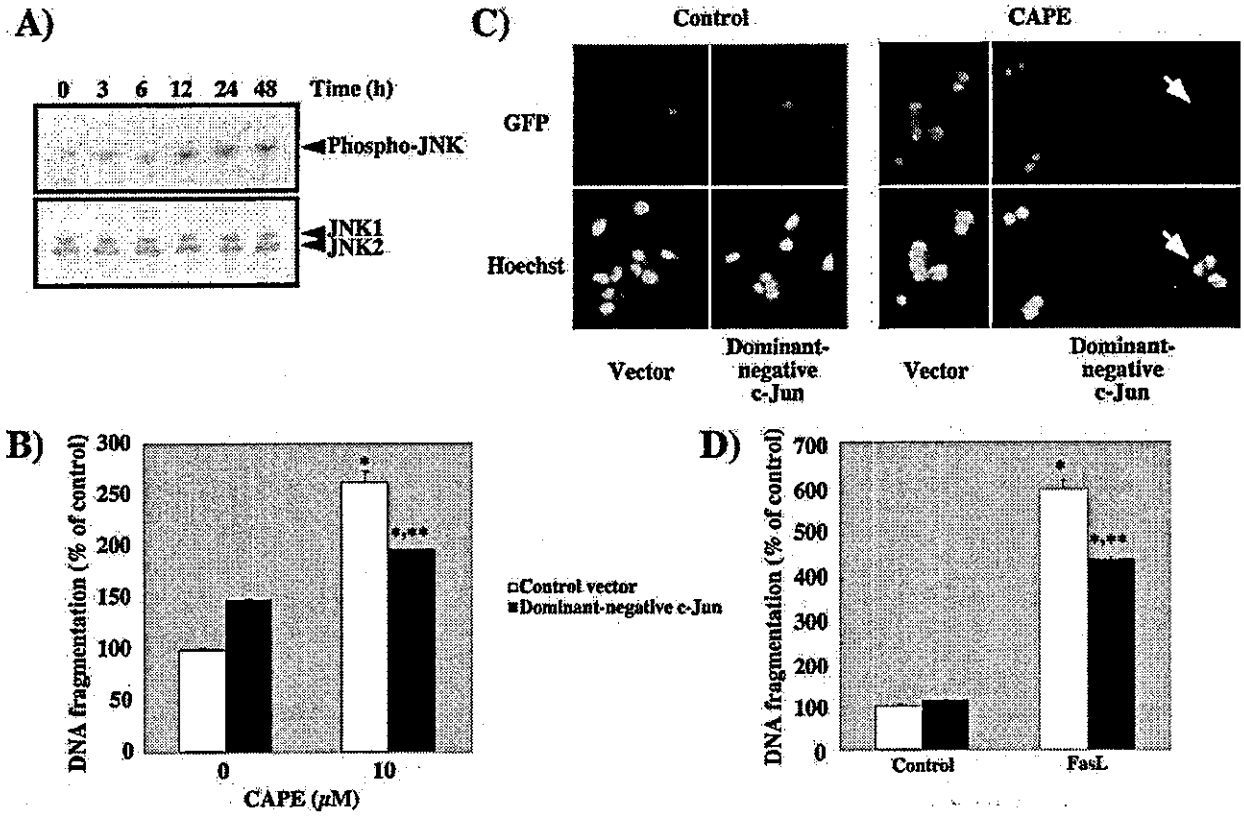

FIG. 4. **JNK involvement in CAPE-induced apoptosis.** *A*, MCF-7 cells were treated with 10 μM CAPE for the indicated times. After cell lysate preparation, immunoblotting analyses were performed using anti-JNK and phospho-JNK antibodies. *B*, MCF-7 cells had been transfected with a control vector, pCMV, or a dominant negative vector, pCMV-Δc-Jun, 24 h before treatment with 10 μM CAPE for 24 h. DNA fragmentation assay was performed as described under "Materials and Methods." Results are presented as the means ± S.E. of three independent experiments. *, $p < 0.05$ compared with control. **, $p < 0.05$ compared with CAPE treatment of control vector. *C*, MCF-7 cells had been co-transfected with pGFP and pCMV or pCMV-Δc-Jun 24 h before treatment with 10 μM CAPE for 24 h. Morphological changes in cells were examined by staining with Hoechst 33258. We considered GFP-positive cells to be pCMV- or pCMV-Δc-Jun-transfected cells. *Arrows* show vector-untransfected cells in a dominant negative c-Jun group (GFP-negative cells). *D*, MCF-7 cells had been transfected with a pCMV or a pCMV-Δc-Jun 24 h before treatment with 5 ng/ml recombinant Fas-L for 24 h. DNA fragmentation assay was performed as described under "Materials and Methods." Results are presented as the means ± S.E. of three independent experiments. *, $p < 0.05$ compared with control. **, $p < 0.05$ compared with Fas-L treatment of control vector.

pendent manner (Fig. 1*A*). To investigate whether or not this decrease in cell viability was caused by apoptosis, we analyzed DNA fragmentation. An increase in histone-associated DNA fragmentation caused by 10 μM CAPE was detected at 12 h and thereafter (Fig. 1*B*). CAPE treatment induced nuclear fragmentation (Fig. 1*C*). These results show that NFκB inhibition by CAPE does induce apoptosis in MCF-7 cells. Moreover, we examined the effects of CAPE on DNA fragmentation in various cell types other than MCF-7. As shown in Fig. 1*D*, CAPE induced apoptosis in adherent cancer cell lines derived from different species such as human hepatocellular carcinoma HepG2 cells and rat myoblastic H9c2 cells but failed to do so in normal human fibroblast WI-38 cells.

CAPE-induced Bax Expression—To investigate the mechanisms underlying CAPE-induced apoptosis, we examined the effect of CAPE on the expressions of apoptosis-related proteins. CAPE treatment markedly decreased the expression of X-chromosome-linked inhibitor of apoptosis, one of the NFκB target genes, after 24 h (Fig. 2*A*), whereas Bax was induced after 12 h of CAPE treatment (Fig. 2*A*). Immunohistochemical analysis revealed CAPE treatment increased the amount of Bax protein in cells, the size of which was reduced by CAPE treatment (Fig. 2*B*, *arrow*).

p38-regulated Bax Induction—Bax is one of the p53 target genes. Because CAPE increased the amount of Bax, we examined the effect of CAPE on p53 transcriptional activity. As shown in Fig. 3*A*, CAPE activated p53 transcription 12 h after CAPE treatment. Because p53 phosphorylation is required for its activation and p53 is directly phosphorylated by certain protein kinases, including p38 which belongs to the MAP kinase superfamily (17, 18), we examined the effect of CAPE on p38 activity by detecting its phosphorylation. CAPE treatment induced p38 activation as early as 6 h; interestingly, this activation preceded the p53 activation (Fig. 3*B*). Moreover, SB203580, a specific p38 inhibitor, partially suppressed CAPE-induced p53 transcriptional activity in a dose-dependent manner (Fig. 3*C*). To investigate whether or not p38 inhibition suppressed the expression of Bax, we examined the effect of SB203580 on Bax expression. SB203580 inhibited CAPE-induced Bax expression (Fig. 3*D*) and CAPE-induced apoptosis (Fig. 3*E*) in a dose-dependent manner. Inhibition of Fas-L-induced apoptosis by SB203580 was also observed in MCF-7 cells (Fig. 3*F*).

JNK Activation by CAPE—JNK, a member of the MAP kinase superfamily, is involved in apoptosis. Because Bax is essential for JNK-dependent apoptosis and JNK is necessary for Bax activation (19, 20), we investigated the effect of CAPE on JNK activity. CAPE treatment induced JNK activation in a time-dependent manner (Fig. 4*A*). Because the mutant (Δc-Jun) lacks the transactivation domain of c-Jun, acts as a dom-

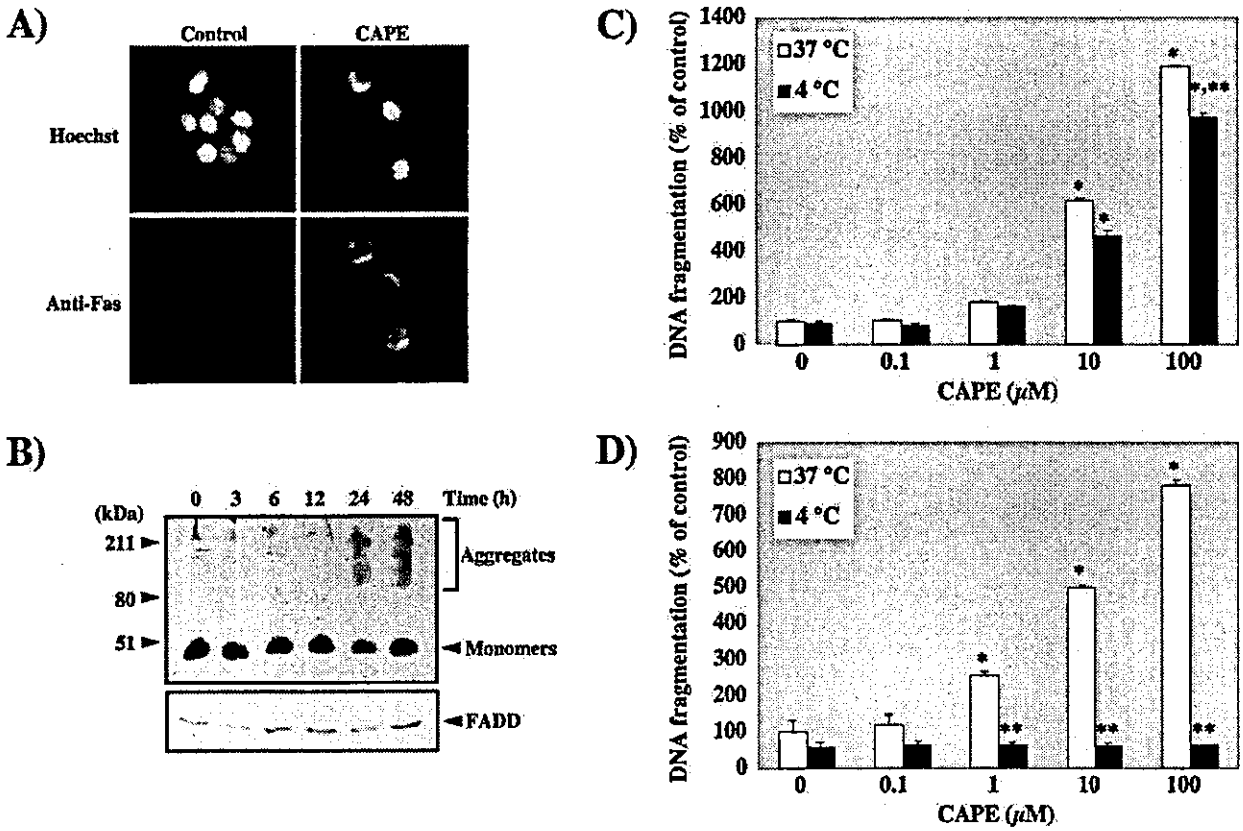

FIG. 5. **CAPE-induced Fas aggregation.** *A*, MCF-7 cells were treated with 10 μM CAPE for 24 h. Intracellular localization of Fas protein was examined by immunofluorescence microscopy. *B*, MCF-7 cells were treated with 10 μM CAPE for the indicated times. After cell lysate preparation, immunoblotting analyses were performed using anti-Fas (*top panel*) and FADD (*bottom panel*) antibodies. *C*, MCF-7 cells were incubated at 4 °C for 30 min, treated with 10 μM CAPE for 1 h at 4 °C, and further incubated for 24 h at 37 °C. DNA fragmentation assay was performed as described under "Materials and Methods." *D*, MCF-7 cells were incubated at 4 °C for 30 min, treated with 10 μM CAPE, and further incubated for 24 h at 4 °C in a high pressure-resistant iron pot that allowed the cells to be maintained under the same air conditions. DNA fragmentation assay was performed as in *panel C*. Results are presented as the means ± S.E. of three independent experiments. *, $p < 0.05$ compared with control. **, $p < 0.05$ compared with 37 °C.

inant negative mutant, and inhibits the JNK-mediated pathway (12), we examined the effect of Δc-Jun transfection on CAPE-induced apoptosis. Δc-Jun expression partially but significantly suppressed CAPE-induced DNA fragmentation (Fig. 4*B*). Moreover, we also performed morphological observations. Nuclear fragmentation was detected in control vector-transfected cells (Fig. 4*C*, GFP-positive cells in the control group). On the other hand, nuclear fragmentation was also detected in Δc-Jun-nonexpressing cells (Fig. 4*C*, GFP-negative cells in the dominant negative group, *arrow*). However, no nuclear fragmentation was detected in Δc-Jun-expressed cells (GFP-positive cells in the dominant negative group) despite CAPE exposure (Fig. 4*C*). The same observation was made in MCF-7 cells undergoing recombinant Fas-L-induced apoptosis (Fig. 4*D*).

Induction of Fas Aggregation by CAPE—We examined the effects of CAPE on Fas, which is a member of the death receptor family and functions upstream from Bax, because death receptor family members cluster, thereby inducing a death signal (21, 22). Using anti-Fas antibody, CAPE caused Fas aggregation in MCF-7 cells (Fig. 5*A*). Because Fas aggregates, which have a high molecular mass and are SDS- and β-mercapto-ethanol-resistant, are immediately formed following receptor cross-linking (23), we estimated the apparent molecular mass of Fas aggregates by immunoblotting analysis (Fig. 5*B*, *top panel*). High molecular mass aggregates formed at 24 h and thereafter when NFκB activity was almost completely inhibited. It was previously reported that maintaining cells at a low temperature blocks Fas receptor clustering by >90% (24, 25). Although the mechanism underlying the low temperature effect is not clear, changes in membrane fluidity have been suggested. It should be noted that keeping cells at a low temperature does not interfere with transcription in general (25). To clarify the role of Fas aggregation in CAPE-induced apoptosis, we preincubated cells at 4 °C and then measured DNA fragmentation. As shown in Fig. 5*C*, short exposure to a low temperature (4 °C) for 1 h with CAPE treatment after preincubation for 30 min at 4 °C slightly suppressed CAPE-induced DNA fragmentation, whereas prolonged exposure at 4 °C for 24 h significantly suppressed CAPE-induced DNA fragmentation (Fig. 5*D*). Because lowering the temperature may affect numerous other processes besides clustering, we confirmed Fas aggregation utilizing other techniques, such as an immunoprecipitation protocol. The basic principle is that a less than stoichiometric amount of antibody will be able to immunoprecipitate more Fas molecules if aggregation occurs after CAPE treatment. In contrast, a sufficient amount of antibody will immunoprecipitate the same amount of Fas molecules regardless of aggregation. At limited antibody concentrations, the amount of immunoprecipitated Fas was increased by CAPE treatment (Fig. 6*A*). As expected, equal amounts of Fas were immunoprecipitated under conditions of antibody excess (Fig. 6*A*). To determine whether this Fas aggregation functions as a Fas death system in NFκB inhibition-induced apoptosis, our attention was drawn to an adapter molecule, FADD, which

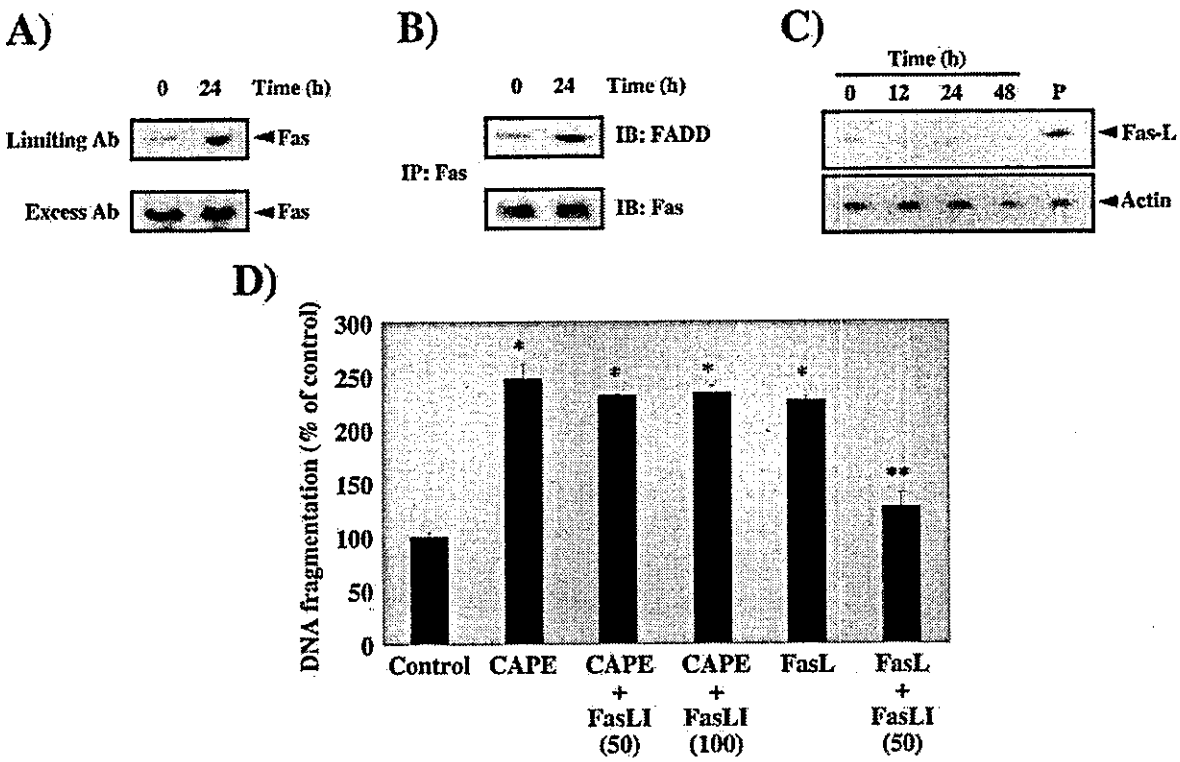

FIG. 6. **Fas-L-independent activation of Fas system by CAPE.** *A*, MCF-7 cells were treated with 10 μM CAPE for 24 h. The cells were treated with a cross-linker, lysed for immunoprecipitation using a Fas-specific antibody under antibody (*Ab*)-limiting conditions (*top panel*) or antibody excess conditions (*bottom panel*) as described under "Materials and Methods." Immunoblot analyses of immunoprecipitates were performed using specific antibodies. *B*, MCF-7 cells were treated with 10 μM CAPE for 24 h. The cells were treated with a cross-linker and lysed, and the extract was used for immunoprecipitation (*IP*). Half of the immunoprecipitate was used for immunoblot analysis to detect the presence of FADD (*top panel*); the other half was used to detect the presence of Fas (*bottom panel*). *C*, MCF-7 cells were treated with 10 μM CAPE for the indicated times. After cell lysate preparation, immunoblot analyses were performed using specific antibodies. *P* denotes a positive control using a whole cell lysate of human chronic myelogenous leukemia K562 cells. *D*, MCF-7 cells were treated with 10 μM CAPE or 5 ng/ml recombinant Fas-L in combination with 50 or 100 μg/ml Fas-L inhibitor (*FasLI*) for 24 h. DNA fragmentation assay was performed as described under "Materials and Methods." Results are presented as the means ± S.E. of three independent experiments. *, $p < 0.05$ compared with control. **, $p < 0.05$ compared with Fas-L alone.

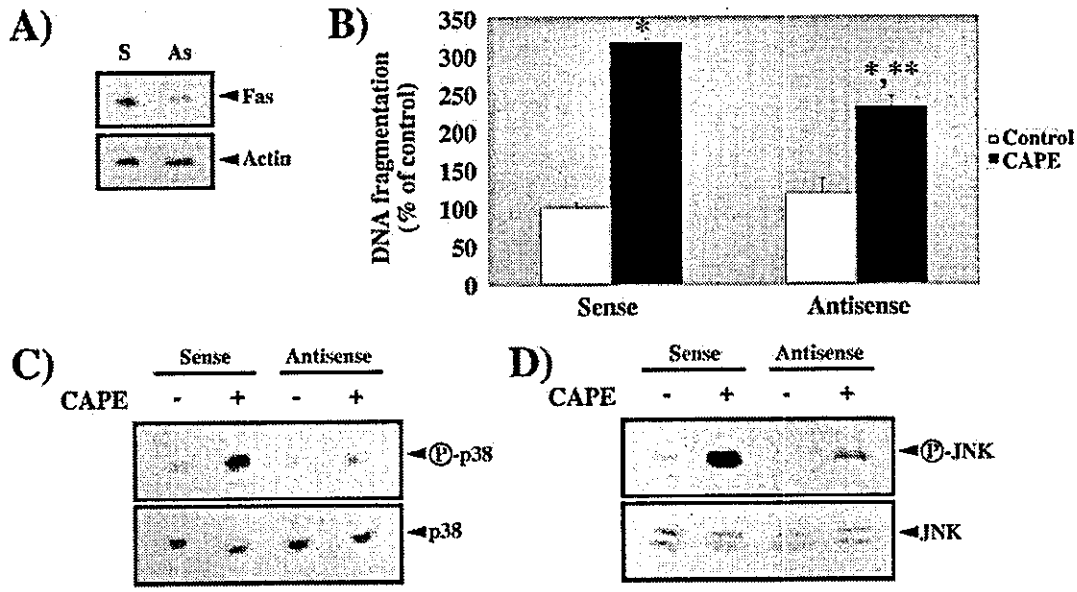

FIG. 7. **Effect of Fas antisense oligonucleotides on CAPE-induced apoptosis.** MCF-7 cells were transiently transfected with sense (*S*) or antisense (*As*) phosphorothioate oligodeoxynucleotides as described under "Materials and Methods." After cell lysate preparation, immunoblot analysis was performed using a Fas-specific antibody (*A*). After being transiently transfected with sense or antisense phosphorothioate oligodeoxynucleotides, MCF-7 cells were treated with CAPE for 24 h. DNA fragmentation assay was performed as described under "Materials and Methods." Results are presented as the means ± S.E. of three independent experiments. *, $p < 0.05$ compared with control. **, $p < 0.05$ compared with CAPE of sense (*B*). After cell lysate preparation, immunoblot analyses were performed using specific antibodies (*panels C* and *D*).

couples the Fas death receptor to procaspase-8. As shown in Fig. 5*B* (*bottom panel*), there was no change in FADD amount with CAPE treatment. To investigate whether CAPE-mediated Fas aggregation resulted in FADD recruitment, co-immunoprecipitation experiments were performed (Fig. 6*B*). Immunoprecipitation of Fas followed by immunoblotting using FADD-specific antibody revealed an increase in the association of FADD with Fas. On the other hand, Fas-L expression in MCF-7 cells remained low, and no change was detectable with CAPE treatment (Fig. 6*C*). To investigate whether or not the multimerization of Fas and Fas-FADD complex formation required Fas-L, we examined the effect of a Fas-L inhibitor on CAPE-induced apoptosis. As shown in Fig. 6*D*, the Fas-L inhibitor effectively inhibited recombinant Fas-L-induced apoptosis. However, the Fas-L inhibitor did not change CAPE-induced apoptosis despite treatment with a concentration higher than that that inhibited Fas-L-induced apoptosis (Fig. 6*D*). We also investigated whether or not Fas really was required for CAPE-induced apoptosis. An alternate approach to knocking out Fas signaling involves transient transfections with Fas antisense oligomers. As shown in Fig. 7*A*, the expression of Fas antisense oligomers significantly decreased Fas compared with Fas sense oligomers. Under these conditions, we investigated the effects of expressing Fas antisense oligomers on CAPE-induced apoptosis. As a result, the expression of Fas antisense oligomers significantly suppressed CAPE-induced apoptosis compared with Fas sense oligomers (Fig. 7*B*). Furthermore, the activation of JNK or p38 induced by CAPE was also inhibited by the expression of Fas antisense oligomers compared with Fas sense oligomers (Fig. 7, *C* and *D*). Consequently, CAPE produces clustering of death receptors, suggesting Fas activation via a Fas-L-independent mechanism. This in turn causes apoptosis via Bax, which is regulated by MAPKs (p38/JNK) and p53.

IκBΔN-induced Fas Activation and Apoptosis—To clarify whether or not the aforementioned results are attributable to the inhibition of NFκB by CAPE, we constructed a truncated form of IκBα (IκBΔN) lacking phosphorylation sites essential for NFκB activation. As expected, CAPE inhibited the transcriptional activity of NFκB in a dose- and time-dependent manner in MCF-7 cells (Fig. 8, *A* and *B*). We confirmed that IκBΔN expression inhibited the transcriptional activity of NFκB in a time-dependent manner, and no NFκB activity was detected at 48 h after AdexIκBΔN infection (Fig. 8*C*). IκBΔN expression in MCF-7 cells significantly increased DNA fragmentation as compared with the lacZ gene (Fig. 9*A*). Under these conditions, Fas aggregation was detected in cells with shrunken nuclei (Fig. 9*B*, *arrow*) and high molecular mass proteins reacted with anti-Fas antibody (Fig. 9*C*). These changes did not occur in LacZ-expressing cells. To determine whether IκBΔN-induced apoptosis requires Fas aggregation, we preincubated cells at 4 °C and then measured DNA fragmentation. Blockade of death receptor clustering at 4 °C significantly inhibited IκBΔN-induced DNA fragmentation (Fig. 9*D*). Moreover, the expression of IκBΔN inhibited X-chromosome-linked inhibitor of apoptosis and induced Bax protein (Fig. 10*A*). Immunohistochemical analysis revealed the amount of Bax protein to be increased by IκBΔN expression (Fig. 10*B*). Thus, IκBΔN expression induced apoptosis by the same mechanism as CAPE.

Requirement of Caspase-8 and -9 for NFκB Inhibition-induced Apoptosis—To further investigate the possible requirements of both Fas aggregation and Bax action in the initiation of NFκB inhibition-induced apoptosis, we examined the effects of caspase-8 and -9 inhibitors. Z-VAD-FMK is an irreversible caspase inhibitor with a broad specificity against various

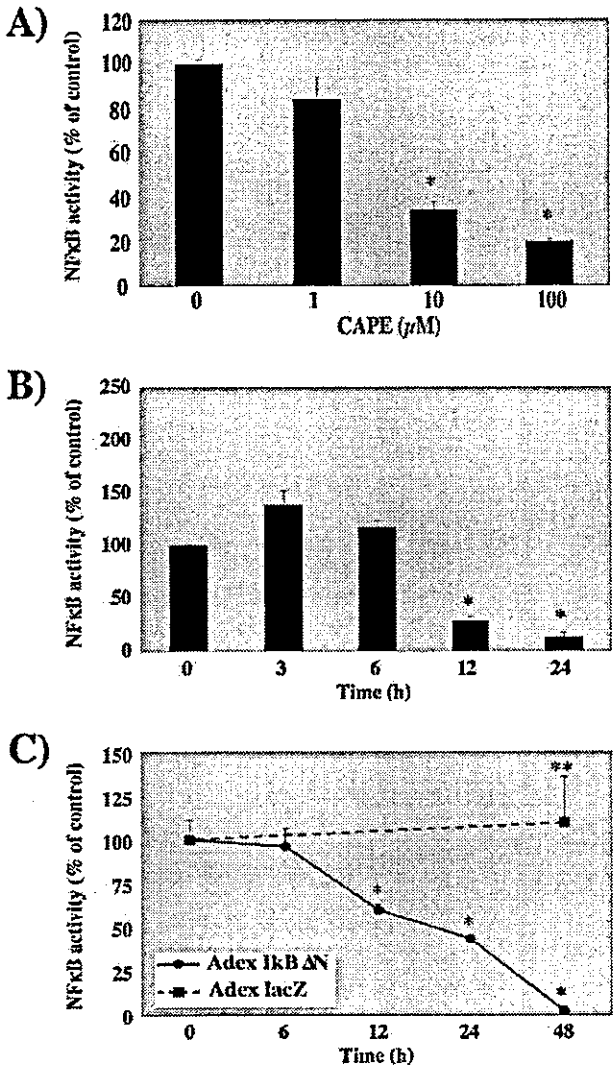

FIG. 8. **Effect of IκBΔN transfection on NFκB activity.** MCF-7 cells were treated with CAPE at the indicated concentrations for 24 h (*A*) or with 10 μM CAPE for the indicated times (*B*). MCF-7 cells were infected with AdexlacZ (m.o.i. = 100) and AdexIκBΔN (m.o.i. = 100). *C*, NFκB transcriptional activity was measured as described under "Materials and Methods." Results are presented as the means ± S.E. of three independent experiments. *, $p < 0.05$ compared with control. **, $p < 0.05$ compared with AdexIκBΔN.

caspases, Z-IETD-FMK is an irreversible specific inhibitor of caspase-8, and Z-LEHD-FMK is an irreversible specific inhibitor of caspase-9. When the cells were pretreated with each caspase inhibitor, DNA fragmentation caused by either CAPE treatment or IκBΔN expression was suppressed in the presence of each caspase inhibitor (Fig. 11). Because treatment with Z-IETD-FMK or Z-LEHD-FMK alone suppressed NFκB inhibition-induced apoptosis, caspase-8 and -9 are considered to be involved in an apoptotic pathway transmitted via NFκB inhibition. Taken together, these results suggest NFκB inhibition in MCF-7 cells induces Fas activation, activates Bax by a JNK/p38-dependent mechanism, activates caspases, and induces apoptosis.

DISCUSSION

In this study, we clarified for the first time that CAPE, known to inhibit NFκB, leads to the clustering of Fas death

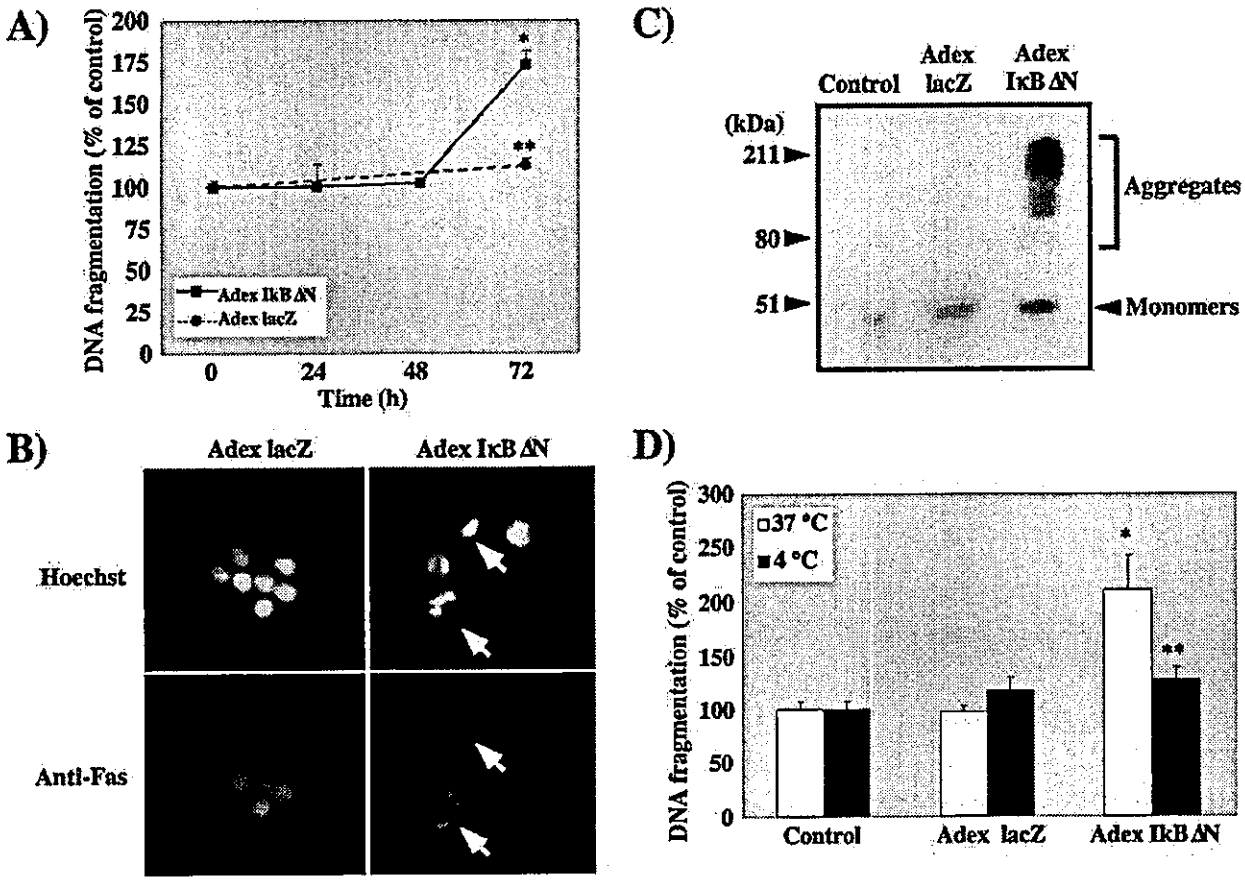

FIG. 9. **IκBΔN-induced apoptosis and Fas aggregation.** MCF-7 cells were infected with AdexlacZ (m.o.i. = 100) and AdexIκBΔN (m.o.i. = 100). *A*, DNA fragmentation assay was performed after the cells had been infected for the indicated times as described under "Materials and Methods." Results are presented as the means ± S.E. of three independent experiments. *, $p < 0.05$ compared with control. **, $p < 0.05$ compared with AdexIκBΔN. *B*, three days after infection, the intracellular localization of Fas protein was examined by immunofluorescence microscopy as described under "Materials and Methods." *C*, three days after infection, cell lysates were prepared and immunoblotting analysis was performed using anti-Fas antibody. *D*, MCF-7 cells were incubated at 4 °C for 30 min, infected with AdexlacZ (m.o.i. = 100) and AdexIκBΔN (m.o.i. = 100), and incubated for 3 days at 4 °C in a high pressure-resistant iron pot as described for Fig. 5. DNA fragmentation assay was performed as in *panel A*. Results are presented as the means ± S.E. of three independent experiments. *, $p < 0.05$ compared with control. **, $p < 0.05$ compared with 37 °C.

receptors by a Fas-L-independent mechanism and induces apoptosis. UV is known to cause Fas death receptor clustering by a Fas-L-independent mechanism (24). We have demonstrated herein a new Fas-L-independent mechanism by which inhibition of NFκB, which controls cell survival, is sufficient to induce Fas aggregation, using IκBΔN.

As a ubiquitous multifunctional signaling system, members of the NFκB family play prominent roles in the cell death/survival balance (26). CAPE, a flavonoid derivative, is a biologically active ingredient of honeybee propolis and strongly inhibits NFκB activation. We have demonstrated that apoptosis is induced by CAPE in various cancer cell lines. However, it is noteworthy that CAPE failed to induce apoptosis in WI-38 cells, not a cancer cell line. We investigated NFκB activities in various cell lines, including those described in this report, and found apoptosis induction by NFκB inhibition to parallel basal NFκB activities (data not shown). Namely, cancer cells with high basal NFκB activity are more sensitive to NFκB inhibition by CAPE than normal cells. This raises the possibility that cancer cell-specific drugs could be developed if NFκB-specific inhibitors were available for humans.

In Fas-mediated cell death, it is well known that Fas binds to its ligand, Fas-L (28, 29). On the other hand, CAPE induced Fas aggregation and activated Fas independently of Fas-L in MCF-7 cells. It is also known that death receptor aggregation results in the activation of two independent signaling pathways. One well characterized pathway involves the death adaptor molecule FADD. The other pathway is mediated through Daxx, which enhances Fas-induced apoptosis by activating the JNK/p38 kinase cascade via apoptosis signal-regulating kinase 1 (30–32), culminating in activation of the Bax subfamily of Bcl2-related proteins (20) or in the phosphorylation and activation of transcription factors such as p53 (17, 18). To clarify the role of these two pathways in CAPE-induced apoptosis, we examined each step. First, treatment with Fas antisense oligonucleotides significantly inhibited CAPE-induced cell death. Second, immunoblotting using FADD-specific antibody clarified the association of FADD with Fas, and caspase-8 inhibitor also inhibited CAPE-induced apoptosis. These results suggest that CAPE promotes Fas aggregation and the association of Fas with FADD and subsequently activates caspase-8. Next, we examined the role of a second pathway using Fas antisense oligonucleotides, a p38-specific inhibitor (SB203580), and dominant negative c-Jun. Treatment with Fas antisense oligonucleotides suppressed CAPE-induced cell death and JNK/p38 activation. SB203580 and dominant negative c-Jun partially but significantly suppressed CAPE-induced p53 activation, Bax expression, and apoptosis. Although we could not exclude the involvement of some pathway other than the Fas system, our results show both FADD/

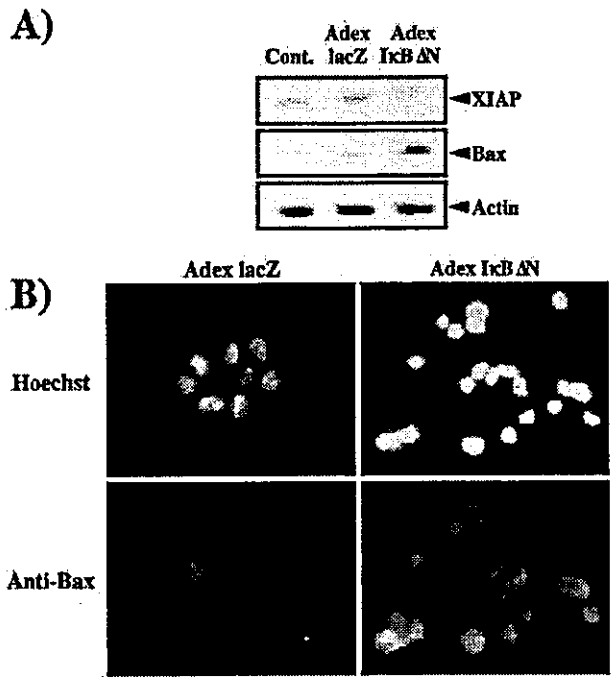

FIG. 10. **Effects of IκBΔN on expressions of apoptosis-related proteins.** MCF-7 cells were infected with AdexlacZ (m.o.i. = 100) and AdexIκBΔN (m.o.i. = 100). *A*, three days after infection, cell lysates were prepared and immunoblotting analyses were performed using specific antibodies. *B*, three days after infection, intracellular localization of Bax protein was examined by immunofluorescence microscopy as described under "Materials and Methods."

caspase-8 and JNK/p38 play important roles in CAPE-induced cell death in MCF-7 cells.

In general, an apoptotic signal can be transmitted through either the death receptors (28, 29) or mitochondria (33, 34). Mitochondria-mediated cell death is distinguished from Fas-mediated apoptosis. Mitochondria sense the apoptotic signal and activate caspase-9 via the release of cytochrome *c* and Apaf-1, ultimately triggering apoptosis. In this study, CAPE induced Fas aggregation and a caspase-8 inhibitor suppressed CAPE-induced apoptosis. However, a caspase-9 inhibitor alone suppressed CAPE-induced apoptosis. These results suggest that both signals are necessary for CAPE-induced apoptosis. As for MCF-7 cells, we speculate that the death signal of caspase-8 activated by the association of Fas with FADD is transmitted to mitochondria via a second messenger such as Bid. Then, p38 activated by Fas aggregation acts on p53, followed by the expression of Bax, which is in turn activated by JNK that is activated by Fas aggregation. Subsequently, cytochrome *c* is released, caspase-9 is activated, and apoptosis is induced via caspases other than caspase-3.

Because a truncated form of IκBα (IκBΔN) lacking the phosphorylation sites essential for NFκB activation is a specific inhibitor of NFκB, we used this approach in addition to CAPE to obtain a line of convincing evidence that NFκB inhibition activates Fas and thereby leads to apoptosis. IκBΔN expression caused a phenomenon qualitatively identical to that observed with CAPE treatment. These results demonstrate that NFκB inhibition accounts for CAPE-induced Fas activation and apoptosis. However, it is still unclear how NFκB inhibition increases Fas aggregation/activation. As Anderson (36) as well as Rosette and Karin (37) reported, it is possible that physical perturbation of the plasma membrane or conformational

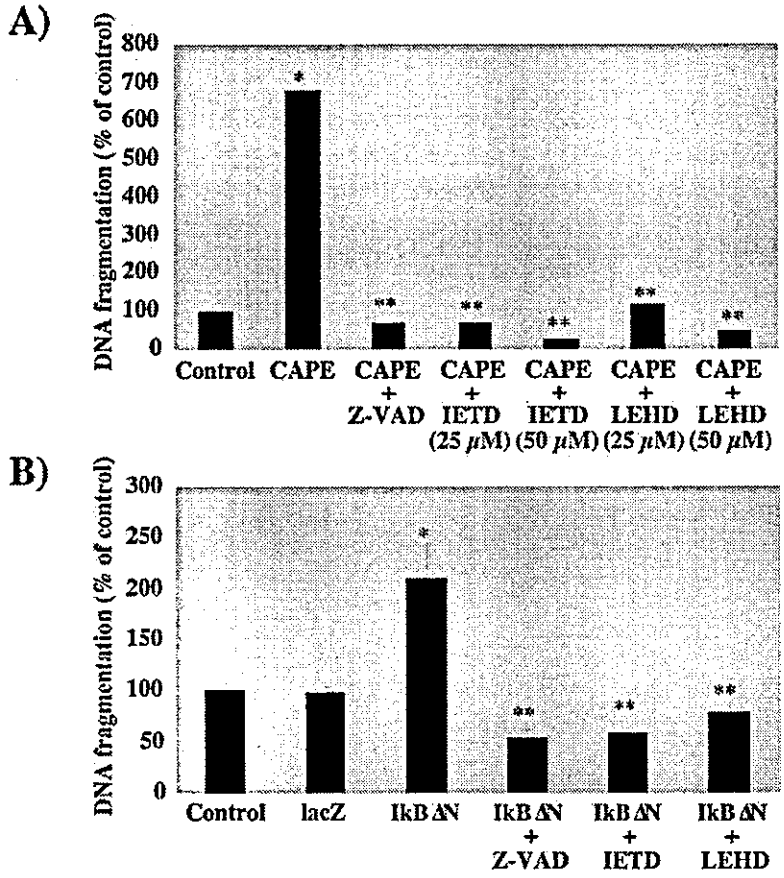

FIG. 11. **Effects of caspase inhibitors on CAPE- and IκBΔN-induced apoptosis.** *A*, after MCF-7 cells had been pretreated with various caspase inhibitors for 30 min at the indicated concentrations, cells were treated with 10 μM CAPE for 24 h. DNA fragmentation assay was performed as described under "Materials and Methods." *B*, after MCF-7 cells had been pretreated with 50 μM of various caspase inhibitors for 30 min, the cells were infected with AdexlacZ (m.o.i. = 100) or AdexIκBΔN (m.o.i. = 100). Three days after infection, DNA fragmentation assay was performed as described under "Materials and Methods." Results are presented as the means ± S.E. of three independent experiments. *, $p < 0.05$ compared with control. *Z-VAD*, *IETD*, and *LEHD* denote Z-VAD-FMK, Z- IETD-FMK, and Z-LEHD-FMK, respectively. **, $p < 0.05$ compared with CAPE alone or AdexIκBΔN alone.

change through expression changes in some proteins via the inhibition of NFκB may cause receptor clustering. From the clinical perspective, it is interesting that CAPE, a natural flavonoid, exerted a stronger effect than IκBΔN in apoptosis induction.

In summary, we have demonstrated that the inhibition of NFκB is pro-apoptotic in human breast cancer MCF-7 cells and that this effect is attributable to Fas death receptor clustering.

Acknowledgment—We gratefully acknowledge the gift of p3xκB-Luc from Dr. R. M. Schmid (Department of Internal Medicine I, University of Ulm).

REFERENCES

1. Bellas, R. E., FitzGerald, M. J., Fausto, N., and Sonenshein, G. E. (1997) *Am. J. Pathol.* **151,** 891–896
2. Hishikawa, K., and Nakaki, T. (2002) *Heart Drug* **2,** 303–311
3. Akira, S., and Kishimoto, T. (1997) *Adv. Immunol.* **65,** 1–46
4. Maniatis, T. (1997) *Science* **278,** 818–819
5. Stancovski, I., and Baltimore, D. (1997) *Cell* **91,** 299–302
6. Zandi, E., Rothwarf, D. M., Delhase, M., Hayakawa, M., and Karin, M. (1997) *Cell* **91,** 243–252
7. Natarajan, K., Singh, S., Burke, T. R., Jr., Grunberger, D., and Aggarwal, B. B. (1996) *Proc. Natl. Acad. Sci. U. S. A.* **93,** 9090–9095
8. Watabe, M., Kakeya, H., and Osada, H. (1999) *Oncogene* **18,** 5211–5220
9. Watabe, M., Masuda, Y., Nakajo, S., Yoshida, T., Kuroiwa, Y., and Nakaya, K. (1996) *J. Biol. Chem.* **271,** 14067–14072
10. Watabe, M., Nakajo, S., Yoshida, T., Kuroiwa, Y., and Nakaya, K. (1997) *Cell Growth & Differ.* **8,** 871–879
11. Watabe, M., Machida, K., and Osada, H. (2000) *Cancer Res.* **60,** 5214–5222
12. Watabe, M., Ito, K., Masuda, Y., Nakajo, S., and Nakaya, K. (1998) *Oncogene* **16,** 779–787
13. Rehemtulla, A., Hamilton, C. A., Chinnaiyan, A. M., and Dixit, V. M. (1997) *J. Biol. Chem.* **272,** 25783–25786
14. Luo, J., Sun, Y., Lin, H., Qian, Y., Li, Z., Leonard, S. S., Huang, C., and Shi, X. (1997) *J. Biol. Chem.* **278,** 4542–4551
15. Hirahashi, J., Takayanagi, A., Hishikawa, K., Takase, O., Chikaraishi, A., Hayashi, M., Shimizu, N., and Saruta, T. (2000) *Kidney Int.* **57,** 959–968
16. Brown, K., Gerstberger, S., Carlson, L., Franzoso, G., and Siebenlist, U. (1995) *Science* **267,** 1485–1488
17. Bulavin, D. V., Saito, S., Hollander, M. C., Sakaguchi, K., Anderson, C. W., Appella, E., and Fornace, A. J., Jr. (1999) *EMBO J.* **18,** 6845–6854
18. Sanchez-Prieto, R., Rojas, J. M., Taya, Y., and Gutkind, J. S. (2000) *Cancer Res.* **60,** 2464–2472
19. Tournier, C., Hess, P., Yang, D. D., Xu, J., Turner, T. K., Nimnual, A., Bar-Sagi, D., Jones, S. N., Flavell, R. A., and Davis, R. J. (2000) *Science* **288,** 870–874
20. Lei, K., Nimnual, A., Zong, W. X., Kennedy, N. J., Flavell, R. A., Thompson, C. B., Bar-Sagi, D., and Davis, R. J. (2002) *Mol. Cell Biol.* **22,** 4929–4942
21. Nagata, S., and Golstein, P. (1995) *Science* **267,** 1449–1456
22. Ashkenazi, A., and Dixit, V. M. (1998) *Science* **281,** 1305–1308
23. Kamitani, T., Nguyen, H. P., and Yeh, E. T. (1997) *J. Biol. Chem.* **272,** 22307–22314
24. Aragane, Y., Kulms, D., Metze, D., Wilkes, G., Poppelmann, B., Luger, T. A., and Schwarz, T. (1998) *J. Cell Biol.* **140,** 171–182
25. Kulms, D., Poppelmann, B., Yarosh, D., Luger, T. A., Krutmann, J., and Schwarz, T. (1999) *Proc. Natl. Acad. Sci. U. S. A.* **96,** 7974–7979
26. Barkett, M., and Gilmore, T. D. (1999) *Oncogene* **18,** 6910–6924
27. Deleted in proof
28. Nunez, G., Benedict, M. A., Hu, Y., and Inohara, N. (1998) *Oncogene* **17,** 3237–3245
29. Enari, M., Talanian, R. V., Wong, W. W., and Nagata, S. (1996) *Nature* **380,** 723–726
30. Yang, X., Khosravi-Far, R., Chang, H. Y., and Baltimore, D. (1997) *Cell* **89,** 1067–1076
31. Chang, H. Y., Nishitoh, H., Yang, X., Ichijo, H., and Baltimore, D. (1998) *Science* **281,** 1860–1863
32. Muromoto, R., Yamamoto, T., Yumioka, T., Sekine, Y., Sugiyama, K., Shimoda, K., Oritani, K., and Matsuda, T. (2003) *FEBS Lett.* **540,** 223–228
33. Li, P., Nijhawan, D., Budihardjo, I., Srinivasula, S. M., Ahmad, M., Alnemri, E. S., and Wang, X. (1997) *Cell* **91,** 479–489
34. Green, D. R., and Reed, J. C. (1998) *Science* **281,** 1309–1312
35. Deleted in proof
36. Anderson, R. G. (1993) *Proc. Natl. Acad. Sci.* **90,** 10909–10913
37. Rosette, C., and Karin, M. (1996) *Science* **274,** 1194–1197

Available online at www.sciencedirect.com
SCIENCE DIRECT®
Biochemical and Biophysical Research Communications 317 (2004) 1103–1107
BBRC
www.elsevier.com/locate/ybbrc

Gene expression profile of human mesenchymal stem cells during osteogenesis in three-dimensional thermoreversible gelation polymer

Keiichi Hishikawa,[a,b,d,*] Shigeki Miura,[c] Takeshi Marumo,[a,b,d] Hiroshi Yoshioka,[c] Yuichi Mori,[c] Tsuyoshi Takato,[d] and Toshiro Fujita[a,b]

[a] *Department of Clinical Renal Regeneration, Graduate School of Medicine, University of Tokyo, Japan*
[b] *Department of Nephrology and Endocrinology, University of Tokyo, Japan*
[c] *Mebiol Inc., Japan*
[d] *Division of Tissue Engineering, The University of Tokyo Hospital, Japan*

Received 8 March 2004

Abstract

This study attempted to characterize the ability of thermoreversible gelation polymer (TGP) to induce differentiation of human mesenchymal stem cells (hMSC) into osteoblasts. Using a long oligo microarray system consisting of 3760 genes, we compared the expression profiles of the cells in 2-dimensional (2D) culture, 3D culture in collagen gel, and 3D culture in TGP with or without osteogenic induction. Compared to 2D culture, the gene expression profile of hMSC showed almost the same pattern in TGP without osteogenic induction, but 72% of genes (2701/3760) were up-regulated in collagen gel. With osteogenic induction, hMSC showed higher ALP activity and osteocalcin production in TGP as compared to 2D culture. Moreover, up-regulation and down-regulation of osteogenic genes were augmented in 3D culture in TGP as compared to 2D culture. As TGP is chemically synthesized and completely free from pathogen such as prion in bovine spongiform encephalopathy, these results suggest that TGP could be applied clinically to induce osteogenic differentiation of hMSC.

Keywords: Stem cell; Osteogenesis; Human mesenchymal stem cell; DNA microarray; Polymer

Human bone marrow mesenchymal stem cells (hMSC) can selectively differentiate into osteogenic, chondrogenic, or adipogenic lineages depending on the conditions of the medium in which they are cultured. When hMSC are cultured with dexamethasone, ascorbic acid-2-phosphate, and β-glycerophosphate, they differentiate into an osteogenic lineage and form mineral [1].

There is a large difference between a flat layer of cells and a complex 3-dimensional (3D) tissue, and the development of biological materials for 3D culture is a key area in regenerative medicine. For 3D culture, many researchers have used collagen gel [2] or "Matrigel" [3], but these materials are prepared from bovine or mouse tumors and are not appropriate for clinical use. To avoid infection in clinical use, chemically synthesized biocompatible polymer is an ideal material. Thermoreversible gelation polymer (TGP) [4] is a biocompatible polymer and is completely free from pathogen such as prion in bovine spongiform encephalopathy [5].

In this study, we examined the osteogenic differentiation of hMSC in TGP and compared comprehensive gene expression with that in a 2D culture system. We report here that osteogenic differentiation was augmented in 3D culture in TGP, and TGP is a potential clinical biomaterial for bone regeneration from hMSC.

Materials and methods

Cell culture. Cryopreserved hMSC from a single donor and their required basal medium and growth supplements were purchased from

* Corresponding author. Fax: +81-3-5800-9738.
E-mail address: hishikawa-tky@umin.ac.jp (K. Hishikawa).

0006-291X/$ - see front matter © 2004 Elsevier Inc. All rights reserved.
doi:10.1016/j.bbrc.2004.03.165

BioWhittaker (Walkersville, MD). Osteogenic medium was also purchased from BioWhittaker. TGP was purchased from Mebiol (Tokyo, Japan). Collagen gel (type I) was purchased from KOKEN (Tokyo, Japan). For TGP preparation, 10 ml of control or osteogenic medium was added to TGP in a T25 flask 24 h before use. On day 0, cells were seeded at a density of 3.0×10^3 cells/cm^2 (2D culture) or 3.0×10^3 cells/ml of TGP (3D culture). The next day, the culture medium was replaced with osteogenic medium, and the medium was changed twice a week until day 14.

Microarray analysis. DNA microarray hybridization experiments were performed using Clontech Atlas glass human 3.8 (BD Bioscience) according to the manufacturer's protocol. The protocol and the complete list of genes can be viewed at http://www.bdbiosciences.com/clontech/techinfo/manuals/index.shtml. The DNA arrays were scanned using GenePix4000A [6].

Measurement of ALP activity, calcium deposition, and osteocalcin. ALP activity was measured using an ALP measurement kit (ALP-K Test; Wako Chemicals) [7]. Osteocalcin was determined using an osteocalcin-immunofluorescence kit (BACHEM AG).

Histochemical staining. After 14 days of culture, cells were washed twice with PBS and fixed with 10% PFA for 10 min at room temperature. Fixed cells were stained with 5% silver nitrate (Nakarai) for von Kossa staining [8].

Results

Microarray analysis in 3D culture

In mammalian tissues, cells connect not only with each other, but also with a support structure called the extracellular matrix (ECM). ECM contains collagen, elastin, laminin, fibronectin, etc., and these proteins contain specific motifs that are particularly favorable for cell attachment and function. On the other hand, TGP contains no such motifs as a scaffold, and nothing is known as to whether this affects cell function or not. When hMSC are cultured in control medium in 2D culture, they slowly proliferate without differentiation. Accordingly, we examined the gene expression profile of hMSC cultured in 3D culture (TGP and collagen gel) in control medium. In TGP culture, scattered plots of gene expression were evenly distributed in both the upper left (1959 genes: 52%) and lower right (1801 genes: 48%) areas. On the other hand, scattered plots of gene

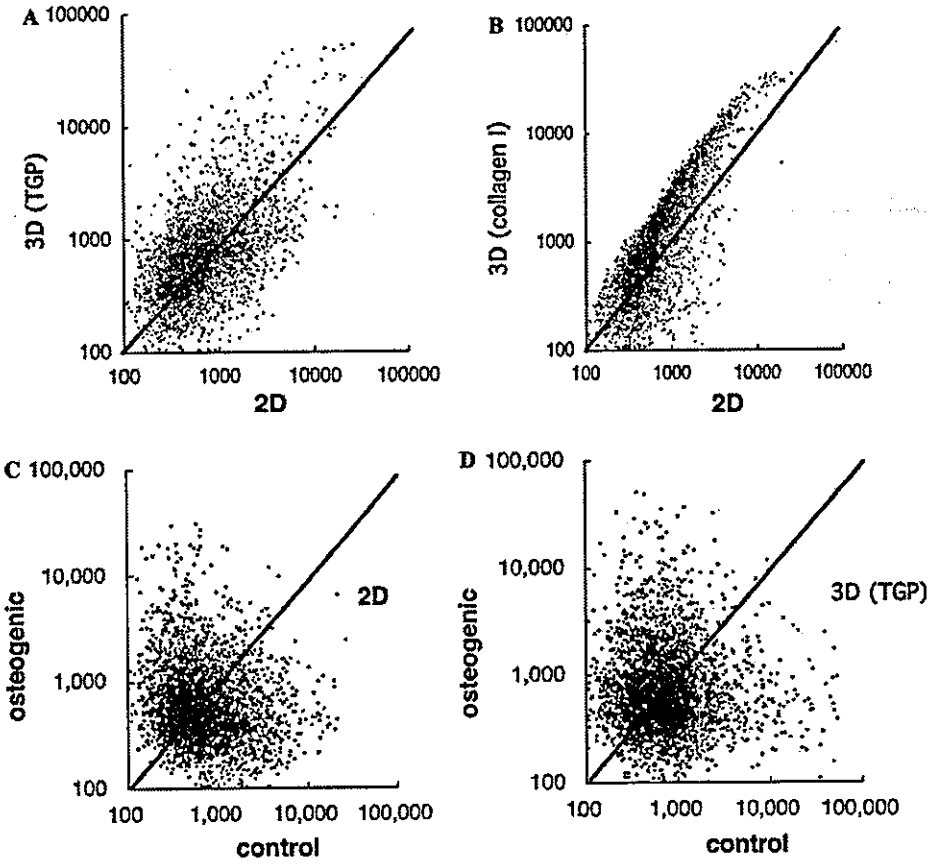

Fig. 1. Scatter-plot analyses of gene expression of hMSC in various culture conditions. (A) 3D culture in TGP vs. 2D culture without induction. (B) 3D culture in collagen gel vs. 2D culture without induction. (C) Osteogenic medium vs. control medium in 2D culture. (D) Osteogenic medium vs. control medium in 3D TGP culture.

expression in collagen gel were mainly distributed in the upper left (2701 genes: 72%), indicating that collagen gel itself stimulated gene expression of hMSC without any induction.

Next, we examined the gene expression profile of hMSC in osteogenic culture medium for 14 days. In 2D culture, unexpectedly, scattered plots of gene expression were evenly distributed in both the upper left (2026 genes: 53.8%) and lower right (1734 genes: 47%) areas, and this was also the case in TGP culture with osteogenic medium (1896 and 1864 genes, respectively).

Matrix mineralization and osteocalcin production

Next, we confirmed whether osteogenic differentiation could be induced in 3D culture in TGP. Human MSC were cultured in 2D or TGP with osteogenic medium for 14 days, and osteogenic differentiation was demonstrated by mineralization stained using the von Kossa method. As shown in Figs. 2A and B, much more mineral was produced in TGP as compared to 2D culture. Moreover, ALP activity [9] and osteocalcin production were significantly higher in TGP as compared to 2D culture (Figs. 2C and D).

Up-regulation and down-regulation of osteogenic genes in TGP

Among 3760 genes, we examined the up-regulation of typical osteogenic genes such as type I collagen [9], alkaline phosphatase [10], osteocalcin [11], and osteopontin [12]. Moreover, recent genome-wide screening by means of a cDNA microarray system consisting of 23,040 genes revealed that 55 genes were up-regulated and 82 genes were down-regulated in hMSC during osteogenic differentiation [13]. We also examined the expression of several of these genes (metallothionetin 2A, osteoprotegrin, dual specificity phosphatase 6,

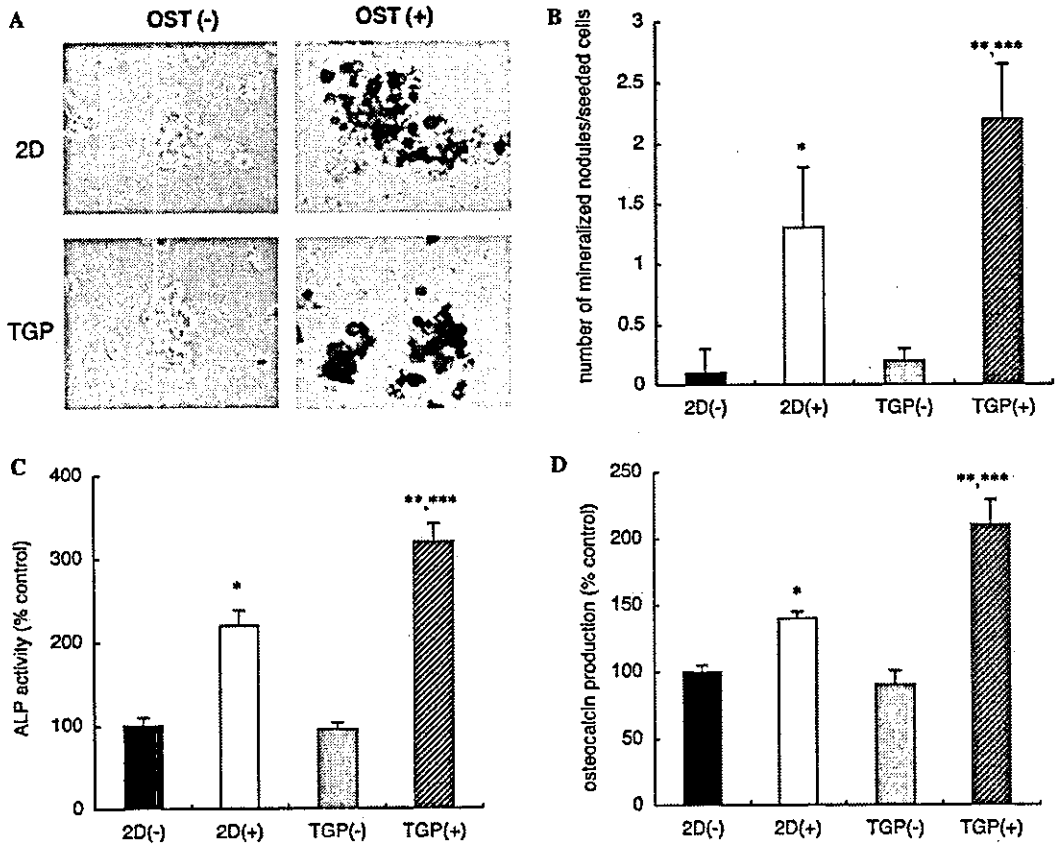

Fig. 2. (A) von Kassa staining without induction (–) and with osteogenic induction (+) in 2D and 3D culture in TGP. (B) von Kossa histomorphometric analysis. Deposition of calcified extracellular matrix (von Kossa staining) was significantly greater with osteogenic induction in both 2D culture and 3D culture in TGP. Deposition was significantly enhanced in TGP compared with 2D culture. (C) Assay for alkaline phosphatase (ALP) activity. ALP activity was significantly higher with osteogenic induction in both 2D culture and 3D culture in TGP. ALP activity was significantly enhanced in TGP compared with 2D culture. (D) Osteocalcin production. Osteocalcin production was significantly higher with osteogenic induction in both 2D culture and 3D culture in TGP. Osteocalcin production was significantly enhanced in TGP compared with 2D culture. $^{*}p < 0.05$: 2D(–) vs. 2D(+). $^{**}p < 0.05$: TGP(–) vs. TGP(+). $^{***}p < 0.05$: 2D(+) vs. TGP(+).

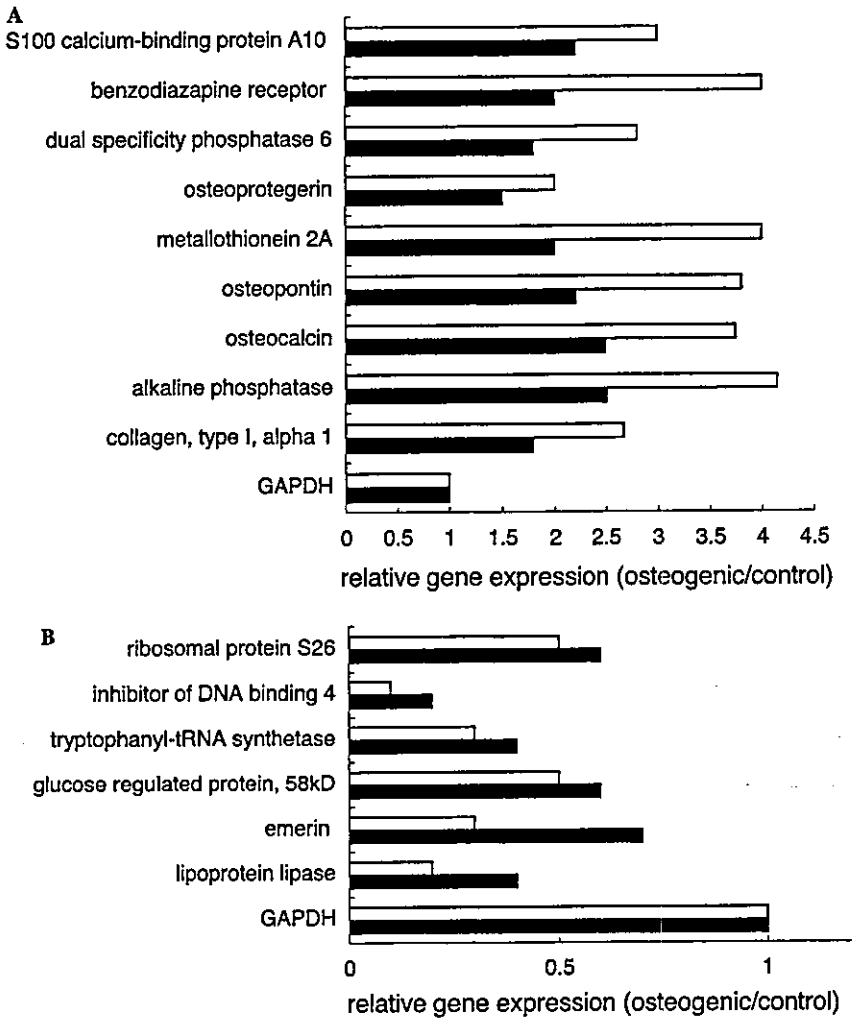

Fig. 3. Osteogenic gene expression in 2D culture and 3D culture in TGP. (A) Genes up-regulated by osteogenic induction. (B) Genes down-regulated by osteogenic induction. Fold change represents the ratio of signal intensity (expression in osteogenic medium/expression in control medium). Closed bars represent 2D culture and open bars represent 3D culture in TGP.

benzodiazapine receptor, S100 calcium binding protein A10, lipoprotein lipase, emerin, glucose-regulated protein 58 kDa, tryptophanyl-tRNA synthetase, inhibitor of DNA binding 4, and ribosomal protein S26) in TGP with osteogenic medium. As shown in Fig. 3, up- or down-regulation of all these genes was augmented in 3D culture in TGP as compared to 2D culture.

Discussion

3D culture techniques are expected to play a key role in regenerative medicine, especially in the field of tissue engineering, but several conditions are required for the culture material. First, it should be free from pathogens such as prion. Collagen gels are usually made from bovine tissue, and it is impossible to rule out the possibility of BSE completely. Matrigel is made from animal tumors. On the other hand, TGP is a chemically synthesized material and completely free from pathogens. Second, to optimize the conditions for lineage-specific differentiation, the material should be able to keep stem cells in an inactive stable condition without induction. Matrigel contains several unidentified growth factors. Collagen gel alone activated gene expression of hMSC without any induction, but TGP did not (Fig. 1). These results suggest that TGP is applicable as a 3D material for clinical regenerative medicine.

Recently, Doi et al. analyzed the gene expression profile during the mineralization process of hMSC by means of a cDNA microarray system consisting of

23,040 genes, and confirmed up-regulation of 55 genes and down-regulation of 82 genes. As shown in Fig. 3, we also confirmed up- or down-regulation of several of these genes during mineralization, but the roles of these genes remain to be determined. It is interesting that ALP activity and osteocalcin production were augmented in 3D culture in TGP compared to 2D culture. During osteogenic induction, it is possible that hMSC may produce some humoral factors that contribute to osteogenic differentiation in an autocrine manner. We speculate that augmentation of osteogenic induction was caused by a high local concentration of these factors with TGP culture. TGP is composed of poly(*N*-isopropylacrylamide-co-*n*-butyl methacrylate) [poly(NIPAAm-co-BMA)] and polyethylene glycol (PEG), and has thermoreversible fine crosslinks between intermolecular poly(NIPAAm-co-BMA) blocks due to hydrophobic interaction [4]. This structure makes it possible to vary the diffusive speed according to the character of the molecules. According to the formula of Lee et al. [14], the diffusive speeds of phenol red (small hydrophilic molecule), myoglobin (large hydrophilic molecule), and methylene blue (small hydrophobic molecule) are calculated as 1.6×10^{-6}, 2.1×10^{-7}, and 7.5×10^{-9} cm^2/s, respectively. Thus, TGP may be able to maintain a high local concentration of hydrophobic molecules and hydrophilic large molecules, and this creates a concentration gradient of each molecule. It is possible that this concentration gradient in TGP may act as a morphogen gradient [15] in vivo and augment osteogenic induction in hMSC.

In summary, 3D culture in TGP is able to maintain hMSC in a stable inactive condition without induction and augment osteogenic differentiation of hMSC cultured with dexamethasone, ascorbic acid-2-phosphate, and β-glycerophosphate. TGP is completely free from prion and may be able to induce a morphogen gradient in the differentiation process in 3D culture. Our results suggest the possible clinical application of TGP for regenerative medicine, especially for bone regeneration by hMSC.

Acknowledgments

This study was supported by a grant from the Open Competition for the Development of Innovative Technology and the Mochida Pharmaceutical Co. Ltd.

References

[1] M.F. Pittenger, A.M. Mackay, S.C. Beck, R.K. Jaiswal, R. Douglas, J.D. Mosca, M.A. Moorman, D.W. Simonetti, S. Craig, D.R. Marshak, Multilineage potential of adult human mesenchymal stem cells, Science 284 (1999) 143–147.

[2] A. Islam, R. Steiner, Primary culture of marrow core in collagen gels: modulation and transformation of endosteal cells. I. Morphologic observations, J. Med. 20 (1989) 241–250.

[3] H.K. Kleinman, M.L. McGarvey, L.A. Liotta, P.G. Robey, K. Tryggvason, G.R. Martin, Isolation and characterization of type IV procollagen, laminin, and heparan sulfate proteoglycan from the EHS sarcoma, Biochemistry 21 (1982) 6188–6193.

[4] H. Yoshioka, M. Mikami, Y. Mori, E. Tsuchida, A synthetic hydrogel with thermoreversible gelation, J. Macromol. Sci. A 31 (1994) 113–120.

[5] S.B. Prusiner, Biology and genetics of prion diseases, Annu. Rev. Microbiol. 48 (1994) 655–686.

[6] K. Hishikawa, B.S. Oemar, T. Nakaki, Static pressure regulates connective tissue growth factor expression in human mesangial cells, J. Biol. Chem. 276 (2001) 16797–16803.

[7] K. Shindo, N. Kawashima, K. Sakamoto, A. Yamaguchi, A. Umezawa, M. Takagi, K. Katsube, H. Suda, Osteogenic differentiation of the mesenchymal progenitor cells, Kusa is suppressed by Notch signaling, Exp. Cell Res. 290 (2003) 370–380.

[8] J.L. Dragoo, J.Y. Choi, J.R. Lieberman, J. Huang, P.A. Zuk, J. Zhang, M.H. Hedrick, P. Benhaim, Bone induction by BMP-2 transduced stem cells derived from human fat, J. Orthop. Res. 21 (2003) 622–629.

[9] M. Sandberg, H. Autio-Harmainen, E. Vuorio, Localization of the expression of types I, III, and IV collagen, TGF-beta 1 and c-fos genes in developing human calvarial bones, Dev. Biol. 130 (1988) 324–334.

[10] G.R. Beck Jr., E.C. Sullivan, E. Moran, B. Zerler, Relationship between alkaline phosphatase levels, osteopontin expression, and mineralization in differentiating MC3T3-E1 osteoblasts, J. Cell. Biochem. 68 (1998) 269–280.

[11] G.S. Stein, J.B. Lian, Molecular mechanisms mediating proliferation/differentiation interrelationships during progressive development of the osteoblast phenotype, Endocr. Rev. 14 (1993) 424–442.

[12] M.A. Dorheim, M. Sullivan, V. Dandapani, X. Wu, J. Hudson, P.R. Segarini, D.M. Rosen, A.L. Aulthouse, J.M. Gimble, Osteoblastic gene expression during adipogenesis in hematopoietic supporting murine bone marrow stromal cells, J. Cell. Physiol. 154 (1993) 317–328.

[13] M. Doi, A. Nagano, Y. Nakamura, Genome-wide screening by cDNA microarray of genes associated with matrix mineralization by human mesenchymal stem cells in vitro, Biochem. Biophys. Res. Commun. 290 (2002) 381–390.

[14] E.K.L. Lee, H.K. Lonsdale, R.W. Baker, E. Drioli, P.A. Bresnahan, Transport of steroids in poly(etherurethane) and poly(ethylene vinyl acetate) membranes, J. Membr. Sci. 24 (1985) 125–143.

[15] J.B. Gurdon, P.Y. Bourillot, Morphogen gradient interpretation, Nature 413 (2001) 797–803.